UNIVERSITÄTSKLINIKUM HAMBURG-EPPENDORF

Zentrum für Experimentelle Medizin der Universität Hamburg

Institut für Angewandte Physiologie

Direktor: Prof. Dr. J. R. Schwarz

Influence of the extracellular potassium concentration on the biophysical properties of KCNQ2, KCNQ3, and KCNQ5 voltage-gated potassium channels

Dissertation

zur Erlangung des Grades eines Doktors der Medizin

an der medizinischen Fakultät der Universität Hamburg

vorgelegt von

Arne Bilet

aus Hamburg

Freie und Hansestadt Hamburg, 2010

Angenommen vom Fachbereich Medizin

der Universität Hamburg am 08.07.2010

Veröffentlicht mit Genehmigung des Fachbereichs

Medizin der Universität Hamburg.

Prüfungsausschuss, die/der Vorsitzende: Prof. Dr. J. R. Schwarz

Prüfungsausschuss, 2. Gutachter/in: Prof. Dr. Christiane Bauer

Prüfungsausschuss, 3. Gutachter/in: PD Dr. R. Bähring

Table of Contents

Figures

Tables

Abbreviations

$[K^+]_e$	Extracellular potassium concentration
cDNA	complementary deoxyribonucleic acid
CHO	Chinese hamster ovary
C_m	Membrane capacitance
C_p	Pipette capacitance
E_K	Potassium equilibrium potential
E_{rev}	Reversal potential
OPA	Operational amplifier
P_O	Channel open probability
P1, P2, P3	pulse intervals (as described in chapter 4.1)
R_f	Feedback resistance
R_g	Seal resistance
R_m	Membrane resistance
R_s	Series resistance
V_c	Command voltage
V_m	Membrane voltage
eGFP	enhanced green fluorescent protein
EC-5, 40, 154K	Extracellular solution containing 5, 40 or 154 mM K^+
IC	Intracellular solution
$V_{1/2}$	Membrane potential of half maximal conductance
k	Slope factor of Boltzmann fit; Membrane potential difference from 1/e (≈37%) to 1-1/e (≈63%) of conductance
τ_{act}	Time constant of activation
τ_{deact}	Time constant of deactivation
KvLQT1-5; KCNQ1-5; Kv7.1-5	
	Different nomenclature used for KCNQ1-5 channel subunits
Vclamp	Clamp potential applied to the membrane by the amplifier
dV	Difference between clamp potential and membrane potential
ITcal	Calculated current amplitude (see chapter 4.4.4)
VTideal,VTreal	Ideal and real tail potentials (see chapter 4.4.4)

1   HYPOTHESIS

Neuronal KCNQ potassium channels have been shown to regulate excitability in the nervous system. Schwarz et al. (2006) have shown that a slow potassium current at the node of Ranvier, I_{Ks}, in large rat sciatic nerve fibres is mediated by KCNQ2 channels. These experiments have shown that there is a shift in voltage dependence of activation of I_{Ks} to more negative potentials with increasing extracellular potassium concentration.

The objective of this investigation is to show whether that shift in the voltage dependence of activation is an intrinsic property of neuronal KCNQ potassium channels by heterologous expression of human homomultimeric KCNQ2 and KCNQ3 in CHO cells.

Furthermore, heteromultimeric KCNQ2+3 and KCNQ3+5 have been shown to underlie the M-current, an important regulator of excitability in the central nervous system. If a negative shift in the voltage dependence of activation can be found for KCNQ homomultimers this might also be true for KCNQ heteromultimers underlying the M-current.

If biophysical properties like the voltage dependence of current activation of the KCNQ-channels are affected by increasing the extracellular potassium concentration this might also be true for other properties such as conductance and time course of activation.

2   INTRODUCTION

In his book „the music of life" the system biologist Denis Nobel has stated that „nature is full of rhythmic mechanisms, varying over an astonishing range of frequencies from over 1000 per second to just once every few years" (Noble 2008). At the short end of this scope lies the basis for the command and control center of animal and human organisms - the central and peripheral nervous system.

Here networks of nerve cells communicate rhythmically via electrochemical circuitry. A fundamental principle that allows this information processing is the electrical excitability of the cell membrane. Driven by ion pumps and transporters an uneven distribution of ions across a semipermeable cell membrane is created (Hille 2001). Ion channels can then rapidly and selectively let ions pass, in the order of 10^7 ions per second (Ashcroft 2006), disrupting the resting membrane potential and generating action potentials, the fundamental currency of bioelectric information computation.

With the decryption of the human genome 262 ion channel subunits have been identified with the group of potassium channels being the most abundant (Venter et al. 2001). Within this group voltage-gated potassium channels have been described as field-effect transistors on a nanometer scale as they can change their conductance in response to fluctuations in the electric field of the cell membrane (Trauner 2009). In parallel to information processing in computers, voltage-gated potassium channels can modulate their output information in the form of ion conductance in relation to their input information of membrane potential. Furthermore, some subtypes of these channels can integrate additional chemical signals by ligand binding or ligand induced signal cascades. For example, the ionic current mediated by KCNQ voltage-gated potassium channels can be decreased by the action of a neurotransmitter on the muscarinic acetylcholine receptors (Delmas and Brown 2005).

KCNQ or Kv7 channels are one of the 12 families of the voltage-gated potassium channels. KCNQ channels are widely distributed through different locations in the brain such as excitatory and inhibitory neurons in hippocampus, chordate nucleus, amygdale and cortex (Ashcroft 2000) as well as through different parts of these neurons, such as dendrites, somata, axons and presynaptic terminals (Cooper et al.

2000; Pongs 2007; Schwarz et al. 2006). Here these channels are a potential pharmacological target for diseases ranging from schizophrenia, anxiety disorders and drug abuse to migraine, neuropathic pain and epilepsy (Brown and Gayle 2009; Hansen et al. 2008; Korsgaard et al. 2005; Munro et al. 2007; Passmore et al. 2003; Porter et al. 2007).

A KCNQ potassium channel is a protein complex composed of pore forming α-subunits KCNQ1-5 each consisting of a 600-1000 amino acid polypeptide chain (Jentsch 2000). Sometimes shorter amino acids are associated to the α-subunits. These β-subunits can further determine the specific channel behavior (Robbins 2001). KCNQ1 can be found in the heart and cochlea (Neyroud et al. 1997). KCNQ4 can be found in the cochlea, vestibular hair cells and the brainstem (Chen and Eatock 2000; Kubisch et al. 1999). KCNQ2, KCNQ3 and KCNQ5 are widely distributed in the central and peripheral nervous system (Jentsch 2000) and will be in the focus of this investigative work. As each channel is composed of four α-subunits a homomultimer can be formed if all four subunits belong to the same subgroup, e.g. KCNQ2. If different subunits assemble, a heteromultimer is formed, e.g. KCNQ2+3. Depending on the subunit composition the voltage-dependent potassium channel has different characteristics in terms of kinetic and pharmacologic properties.

Neuronal KCNQ channels appear to be the molecular correlate of the M-current (Wang et al. 1998). Characteristic for this current is its activation at subthreshold potentials, showing little inactivation and generating a steady voltage-dependent outward current. This current assists in stabilizing the resting membrane potential in the presence of depolarizing currents (Brown and Gayle 2009). The activation of this current by depolarization is relatively slow but steady and can attenuate repetitive action potential discharges acting as a "break" in regulating neuronal excitability (Pongs 2007). This control on neuronal excitability can be modulated by the action of neurotransmitters acting on its receptors such as the muscarinergic acetylcholine receptor - hence its name M-current. This can selectively adapt the frequency of action potentials by releasing the "break" and turn neurons from phasic to tonic firing (Delmas and Brown 2005) - i.e. changing the rhythmicity of information processing. Furthermore, in conditions where the KCNQ channel protein and its function in

regulating neuronal excitability is deficient a hereditary form of epilepsy can arise called benign familial neonatal convulsions (BFNC) (Jentsch 2000).

Investigations at the node of Ranvier in sciatic nerves have shown that I_{Ks}, a slowly activating and deactivating K^+ current, is mediated by KCNQ2 channels (Schwarz et al. 2006). During this investigation the voltage dependence of activation of I_{Ks} was shifted in rising extracellular potassium concentration $[K^+]_e$. A change of $[K^+]_e$ from 10 mM to 160 mM shifted the activation curve by 25 mV to more negative potentials.

$[K^+]_e$ is normally tightly regulated in the brain by the neuron surrounding glial cells (Kuffler et al. 1966; Orkand et al. 1966). Normal values of 2.5-5 mM can rise under conditions of hyperactivity of neurons, during epileptic seizures, and extreme neuronal firing up to a "ceiling value" of 10 mM (Benninger et al. 1980; Heinemann and Dietzel 1984; Heinemann and Lux 1977; Xiong and Stringer 1999). A more important rise in $[K^+]_e$ of up to 50-80 mM has been described for pathophysiologic conditions in spreading depression (Kager et al. 2000; Somjen 2001; Somjen 2002) and brain ischemia (Leis et al. 2005).

As the KCNQ current is important in the control of neuronal excitability and I_{Ks} in the node of Ranvier has shown to be $[K^+]_e$ sensitive, the research question of this investigation is to find out whether $[K^+]_e$ changes the biophysical properties of KCNQ2-, KCNQ3- and KCNQ5-mediated ion currents. Three biophysical properties of KCNQ current are investigated in rising $[K^+]_e$: voltage dependence of activation, kinetics of activation and deactivation, and whole cell conductance. In order to look at KCNQ currents in isolation from all the other ion currents mediated by other channels present in neurons, KCNQ cDNA is introduced into a Chinese hamster ovary (CHO) cells by transfection. These cells then express the KCNQ channel protein selectively and incorporate functional ion channels into their cell membrane. The resultant KCNQ ion current is then accessible to experimental investigation. The method used in order to investigate these heterologously expressed KCNQ channels is the whole cell mode of the patch-clamp technique (Hamill et al. 1981). This allows the experimenter to control and change the membrane potential of the cell and to measure the current over time in order to find out if changes occur in different $[K^+]_e$.

3   METHODS

3.1   Cell culture

The Chinese hamster (Cricetulus griseus) ovary cell line (CHO) resembles mammalian epithelium. This cell line was used as an established mammalian expression system (Puck et al. 1958) for the heterologous expression of KCNQ channels (Selyanko et al. 2001).

CHO cells were cultured in a 50 ml flask (Nunc) in an incubator (Heraeus) at 37°C with a relative humidity of 95% and 5% CO_2. Three times a week the cell culture was separated from its medium (**table 1**), exposed to 2 ml trypsin- EDTA for 3 minutes and then placed in 4 ml of a fresh medium. This separated the confluent cell layer from the base and allowed for cell-splitting. 5 x 10^5 cells (counted in a Neubauer chamber) were suspended in 10 ml fresh medium in a new flask.

For electrophysiological experiments cells were diluted to a concentration of 10^5 cells per ml. These cells were then added onto a glass plate (Eppendorf) that was covered with 100 µl Poly-L-Lysine several minutes before. The cells were allowed to settle for 10 minutes. 2 ml of medium was then added to the preparation. The cells were then incubated for 24 hours before transfection.

Table 1: Composition of CHO culture medium
The medium consisted of the first three constituents in the given percentages and two antibiotics.

89.5 %	MEM alpha medium (Gibeco)
10 %	FCS – fetal calf serum (Roche)
0.3 %	L-glutamine (Sigma)
1 U/ml	Penicillin (Sigma)
1 µg/ml	Streptomycin (Sigma)

3.2   Heterologous expression

24 hours after splitting CHO cells were co - transfected with cDNA of human KCNQ and enhanced green fluorescent protein (eGFP-N1pcDNA3 – Clontech) cDNA using Lipofectamine 2000 system (Invitrogen). Human KCNQ2 (AF110020) and human

KCNQ3 (AAC96191) in pcDNA3 vector (Invitrogen) were a kind gift of Prof. Olaf Pongs. Human KCNQ5 (BC050689) in pcDNA3 vector was a kind gift of Prof. Thomas Jentsch.

EGFP is a 238 amino acid protein originally isolated from the jellyfish Aequorea victoria that fluoresces green when exposed to blue light of 485 nm wave length. Here co-transfection of eGFP with the KCNQ ion channel was used to localise cells that were successfully transfected as shown in **fig. 1**. Out of the cells that showed green fluorescence after 18 hours almost all also showed measurable KCNQ currents.
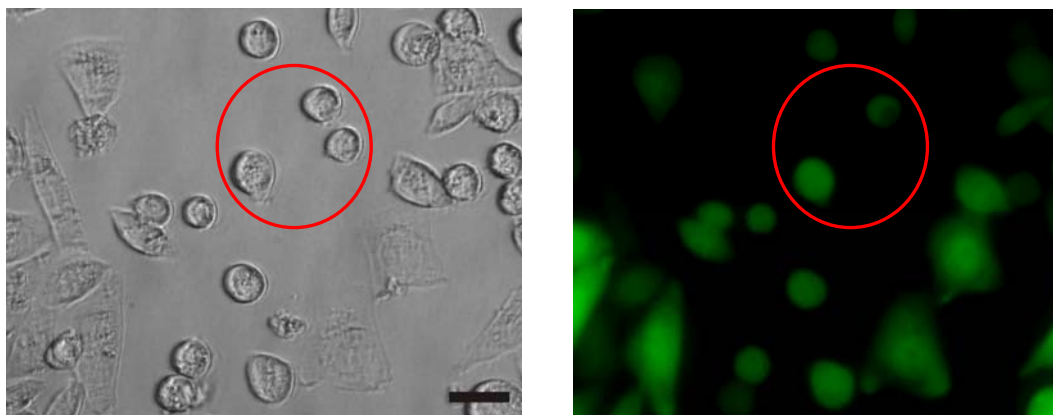
Fig. 1: CHO cells under phase contrast and UV-light microscopy
Population of cultured CHO cells 20 hours after transfection with KCNQ and eGFP cDNA viewed by phase contrast microscopy (*left*) and under ultraviolet light (*right*). Cells showing green fluorescence were successfully transfected with eGFP and used for patch-clamp experiments expecting them to also express functional KCNQ channels. Inside the red circle there are three CHO cells two of which express eGFP. Scale bar represents 20 µm.

For transfection of one culture dish cDNA of KCNQ and eGFP was added to 100 µl Optimem in a 1.5 ml tube. 1.5 µl lipofectamine was diluted in 100 µl optimem in another 1.5 ml tube. Then the content of both tubes was mixed and whirled briefly in a vortex machine.

Thereafter the medium was removed from the cell culture dish and 800 µl Optimem were added onto the CHO cells. After 30 min in the incubator the 200 µl mixture of cDNA, lipofectamine and optimem was added to the cell culture dish and incubated for 3 hours at 37°C. The transfection solution was then removed and new culture medium was added. After an incubation period of 18-27 hours the transfected cells were used for electrophysiological experiments.

Different concentrations of KCNQ subunit cDNA were used for transfection in order to obtain steady-state K^+ currents below 3 nA. cDNA concentrations are given in **table 2**. 0.5 µg of eGFP cDNA was added to every transfection mixture.

Table 2: cDNA concentrations for transfection per 35 mm culture dish
The amount of cDNA in µg is given for each KCNQ subunit for the transfection.

KCNQ subunit	2	3	5	2+3	3+5
cDNA for transfection / µg	0.5	0.5	1.0	0.03, 0.03	1.0, 1.0

3.3 Electrophysiology

3.3.1 Voltage clamp

The investigation of electrical properties of cell membranes has been advanced by the patch-clamp technique (Hamill et al. 1981; Marty and Neher 1983). In order to examine currents mediated by ion channels in the membrane one needs to have good electrical access to the cell under investigation.

In patch-clamp investigations one Ag/AgCl electrode in the bath solution creates access to the extracellular space and is connected to ground potential. The other Ag/AgCl electrode gains electrical access to the intracellular part of the cell via a glass pipette attached to the membrane (**fig. 2**). The pipette often containing a solution similar to intracellular conditions is tightly connected to the surface of the membrane by applying a negative pressure inside the pipette after touching the membrane. This tight seal has an electrical resistance R_g of more than 1 GΩ with respect to the extracellular environment. Electrical access to the inside of the cell is achieved by rupturing the membrane patch under the pipette. Alternatively, one may apply chemicals such as Nystatin to the intracellular solution in order to make the membrane patch permeable to ions (perforated patch) creating electrical access to the cell interior without much disruption of the intracellular protein concentrations.

When investigating the properties of voltage-gated ion channels such as KCNQ one would like to observe the characteristics of ionic current changes with changing the voltage across the membrane V_m. This is possible with patch-clamp experiments in voltage-clamp mode where the membrane voltage is controlled by injecting current

through the electrodes. A simplified sketch of such a circuit (Numberger and Draguhn 1996) can be seen in **fig. 2**. If the seal resistance R_g is much higher than the membrane resistance R_m, the membrane voltage V_m can be clamped to a command voltage V_c very quickly after electronically compensating for the internal resistance of the cell access or series resistance (R_s compensation), the capacitance of the pipette C_p (Cfast-compensation) and the capacitance of the cell membrane C_m. Series resistance R_s was electronically compensated for by 70-90%.

If the command voltage V_c is changed in order to hold the membrane at a different potential or if the conductance of the membrane G_m ($=1/R_m$) changes, as ion channels open or close, the operational amplifier OPA recognizes the difference between its input voltage V_m and the command voltage V_c and injects current via its output through the feedback resistance R_f back into the pipette until the membrane potential equals the command potential. The time course of this current can be measured and equals the current across the membrane. This creates the opportunity to observe the time course of currents through voltage-gated potassium channels like KCNQ.
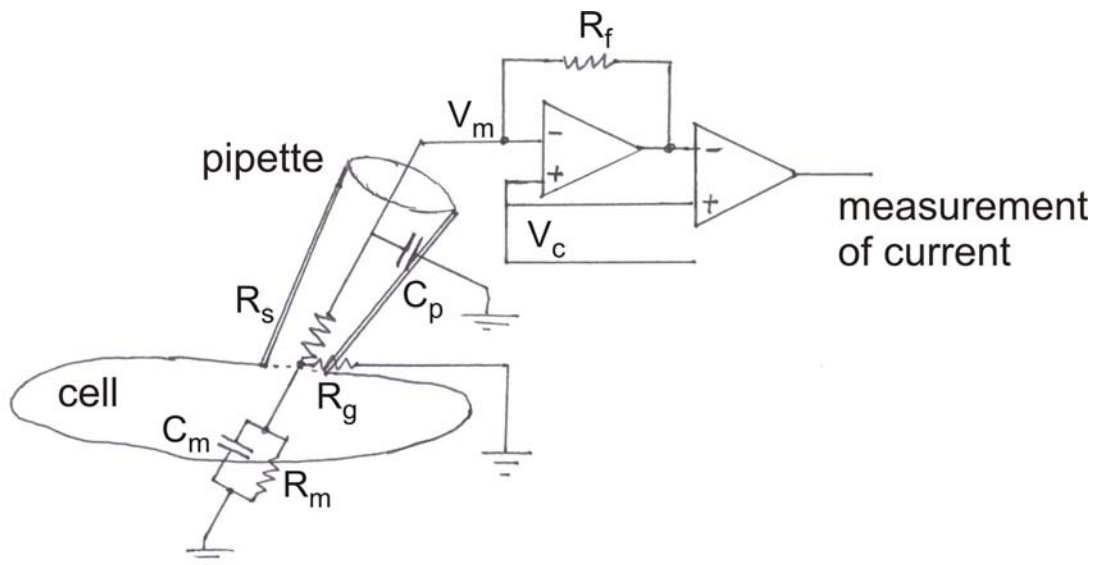
Fig. 2: Schematic circuit diagram of a patch-clamp setup
Passive electrical properties of the cell membrane are represented by a RC circuit element at the bottom of the cell. C_m *membrane capacitance*, R_m *membrane resistance*, R_g *seal resistance*, R_s *series resistance*, C_p *pipette capacitance*, V_m *membrane voltage*, R_f *feedback resistance*, V_c *command voltage* (modified from Numberger und Draguhn, 1996)

3.3.2 Workstation

Microscope (Axiovert 35, Zeiss), micro manipulators (Patchman, Eppendorf) and patch-clamp setup were placed on an antivibration table (Phonotherm Rich.

Thienhaus GmbH) and were shielded from electromagnetic interference by a faraday cage. Green fluorescence in eGFP expressing cells was excited by a mercury vapour lamp with a 485 nm filter (filter set 08, Zeiss).

Data was recorded and analysed using patch-clamp amplifier (EPC-9, HEKA) and Pulse/PulseFit software (v8.65 HEKA) on a personal computer.

Experiments were performed at room temperature 22-25°C.

3.3.3 Glass pipettes

Capillaries made of borosilicate glass (Vitrex GB150T-8P, Science Products GmbH) were pulled and polished into patch pipettes with an automatic electrode puller (DMZ Universal Puller, Zeitz-Instrumente GmbH). The internal resistance of the pipettes when filled and inserted into the bath solution were between 2.0 - 3.5 MΩ (opening diameter between 0.5-1µm).

Bath electrodes consisted of a silver pellet connected to the bath solution via an agar bridge (5% Agar in 150 mM NaCl) inside a curved glass capillary.

3.3.4 Solutions and chemicals

The composition of extracellular and intracellular solutions is described in **table 3**. Extracellular solutions (EC) containing 5 and 154 mM $[K^+]_e$ were prepared. Extracellular solutions containing 40 and 80 mM $[K^+]_e$ were mixed from EC-5 and EC-154 in a ratio of 116:35 and 76:75, respectively. An increase in osmolarity when increasing $[K^+]_e$ was prevented by reducing the concentration of NaCl.

Nystatin was prepared to create a perforated patch with concentrations as described by Horn and Korn (1992). A Nystatin stock solution (60 mg/ml) was prepared by adding 6 mg Nystatin to 100 µl Dimethylsulfoxide (DMSO; Sigma) and carrying out sonification for 30 seconds at maximum intensity (sonificator: Bandelin electronic UW-60). Aliquots of 4 µl were then stored at -20°C. On the day of the experiment, 1 ml intracellular solution (IC) was added to a 4 µl aliquot at the day of experimentation. This was mixed by ultrasound (Bandelin electronic UW-60) for 10 seconds to gain a Nystatin end concentration of 0.24 mg/ml before the measurement. This solution was then stored on ice and in darkness no longer than 6 hours until used to backfill the patch pipette (Horn and Korn 1992).

Table 3: Ion composition of solutions used in experiments

Ion concentrations are given in mM. EC-5 extracellular bath solution with 5 mM K^+ (Ringer), EC-154 extracellular bath solution with 154 mM K^+, EC-40 containing 40 mM K^+ and 111 mM Na^+ was gained from adding together EC-5 and EC-154 in a ratio of 116:35, EC-80 containing 80 mM K^+ and 73 mM Na^+ was mixed from EC-5 and EC-154 in a ratio of 76:75.

Name:	EC-5	EC-154	IC
KCl	5	148	140
K^+ after pH correction	5	154	156
NaCl	140	0	0
Na^+ after pH correction	145	0	0
$MgCl_2$	1	1	2
$CaCl_2$	1	1	1
HEPES	10	10	10
Glucose	5	5	0
EGTA	0	0	2.5
Initial pH	pH 5.5	pH 5.21	pH 3.14
Amount NaOH/KOH added for pH = 7.35	5 NaOH	6 KOH	16 KOH

3.3.5 Liquid junction potential

Liquid junction potentials appear at interfaces between different solutions due to different mobilities of ions (Barry and Lynch 1991). In a patch-clamp experiment the patch pipette contains K^+ as its major positive ions whereas the bath solution contains Na^+. The two major positive ions have different mobilities in solution, $1.96*10^{-5}$ cm^2/s for K^+ and $1.33*10^{-5}$ cm^2/s for Na^+ (Hille 2001). When the patch electrode enters the bath solution K^+ ions tend to diffuse out of the pipette faster than Na^+ ions enter the pipette, creating a positive potential of the bath with respect to the pipette at this liquid junction. This principle is true for all ions at a liquid junction with different concentrations of ions not only between patch pipette and bath but also between bath electrode and bath.

Normally an offset potential was corrected using the HEKA Pulse Software before attaching the pipette tip to the cell membrane and forming a seal. This offset correction compensates for the sum of all offset potentials, including liquid junctions, electrochemical junctions and possible headstage-potentials. When the patch pipette is then attached to the cell membrane the liquid junction is gone but the software

continues to subtract this potential. Therefore a liquid junction potential error has to be taken into account when clamping the cell to a certain voltage especially if this error changes with exchanging solutions.

Liquid junction potential errors were corrected offline by a value measured for liquid junction potentials in different $[K^+]_e$. This liquid junction potential was measured between different bath solutions and patch pipette (Ng and Barry 1995). A glass pipette containing 3 M KCl was used as a bath reference electrode. Then the patch pipette filled with IC solution was entered into the bath containing the same IC solution and the voltage was set to 0 mV potential by the patch-clamp software offset correction. The bath solution was then changed to the different extracellular solutions used in the experiments and the potentials were recorded. Liquid Junction potentials relative to IC solution were measured: -4 mV for EC-5, -3 mV for EC -40, -2 mV for EC-80 and 0 mV for EC-154.

In the following text "pipette potential" describes the potential given by the HEKA amplifier and Pulse software whereas "membrane potential" is the pipette potential corrected for the liquid junction potential.

3.3.6 Experimental procedure

18-27 hours after transfection the glass plate with cells cultured on it were taken out of the medium and put into a culture dish (Nunc) filled with excess 5 mM K^+ extracellular ringer solution (EC-5K) for washing off the medium. Then the CELLocate® disc was placed in a third culture dish for measurement. It was filled with new 5 mM K^+ extracellular bath solution (EC-5K) and placed under the microscope of the patch-clamp setup. The bath electrode was inserted in the dish via an agar bridge. The patch electrode was tip-filled by inserting it into the filtered intracellular solution (IC) without Nystatin for five seconds. The patch pipette was then backfilled with 10 µl of IC containing Nystatin. Air bubbles inside the pipette were removed by tapping. The patch electrode was then fixed to the headstage connected to the micro-manipulator. Before entering the bath solution, a positive pressure of approximately 1 cm water column was applied to the inside of the pipette. After entering the pipette into the bath solution, offset potentials were compensated for with the "set-up" procedure of the "Pulse"–software. The pipette tip was then brought near the cell membrane. The positive pressure inside the pipette was released in order to attach the pipette tip to the cell membrane. Negative pressure

was then applied to the pipette in order to allow a good electrical access to the cell. The measurement was not continued if the seal resistance (R_g) was below one GΩ. After approximately 10-20 min the access or series resistance R_s fell below 15 MΩ by the insertion of Nystatin pores into the cell membrane under the patch pipette. R_s was relatively constant between 5-15 MΩ and was electronically compensated for by 70-90%. Measurements were not conducted with series resistances exceeding 15 MΩ or R_s-compensation below 70%.

The cell membrane was then clamped to a holding potential of -70 mV and pulse protocols were applied. The bath solution was exchanged increasing from 5 mM $[K^+]_e$ to 40 mM by adding 10 ml of new solution (20 times the volume in the dish) with constant removal of fluid by a suction pump. The same pulse protocols were then applied as in low $[K^+]_e$ after compensating slow and fast capacitances again before every series. $[K^+]_e$ was then increased even further (80 mM, 154 mM) before changing back to 5 mM $[K^+]_e$ for control.

Changes in Liquid Junction potential were not compensated for directly but considered in offline analysis.

3.3.7 Data analysis

The data were analysed using Pulse, Pulsefit (HEKA Elektronik, Lambrecht, Germany), Igor Pro 4.0 (Wavemetrics, Lake Oswego, OR, USA) and Excel (Excel, Microsoft, Redmond, WA, USA) data handling and graphical presentation software packages.

Student's t-test performed with Microsoft Excel was paired, two sided and results are presented as mean ± standard error of mean, unless otherwise specified.

Voltage dependence of activation was obtained in two different ways: from tail currents and by conversion of steady-state current to conductance.

Voltage dependence of activation data obtained from tail currents was fitted by a Boltzmann function:

$$\frac{I}{I_{max}} = \frac{1}{1 + e^{\frac{V_{1/2} - V_m}{k}}},$$

where I is the tail current recorded at -100 mV after a pre-pulse to variable membrane potentials. Tail current amplitude was recorded directly after the capacitive peak. I_{max} is the maximum current generated by Igor Pro best sigmoid fit to the data.

$V_{1/2}$ is the membrane potential at which I is 50% of I_{max}. k is the slope factor of sigmoid Boltzmann fit and describes the membrane potential difference from 1/e ($\approx$37%) to 1-1/e ($\approx$63%) of normalized tail current.

Whole-cell conductance was determined from the quotient of the steady-state current at the end of the variable voltage pulse and the potential difference between membrane potential V_m and E_K. Derived from Ohm's law whole-cell conductance G equals the reciprocal of membrane resistance R or the quotient of membrane current I and the ion driving potential. In theory the ion driving potential for an isolated membrane system containing K^+ selective ion channels is the difference between the membrane potential V_m and the potassium equilibrium potential E_K. E_K can be obtained from Nernst's equation.

$$G = \frac{I}{V_m - E_K} \qquad \text{and} \qquad E_K = -\frac{R*T}{z*F} * \ln \frac{[K^+]_i}{[K^+]_e}$$

In Nernst's Equation: the universal gas constant is R=8.32 J K^{-1} mol^{-1}, T is absolute temperature in Kelvin, z is the valency of the K^+ ions (+1); Faraday constant F=9.65×10^4 C mol^{-1}, $[K^+]_i$ and $[K^+]_e$ are intracellular and extracellular potassium concentrations.

E_K calculated from the ion concentrations in the solutions was used as an estimate for conversion of measured currents into conductance. Further details in determining conductance curves for KCNQ and data handling are described as part of results in chapter 4.3.3. The conductance G was then plotted against the membrane potential V_m and fitted with a sigmoid Boltzmann function as described above.

Activation and deactivation kinetics were fitted by single exponential functions (Suh and Hille 2007):

$$\text{Activation: } I(t) = I_{\min} + I_{\max} * (1 - e^{\frac{-t}{\tau_{\text{act}}}}),$$

$$\text{Deactivation: } I(t) = I_{\min} + I_{\max} * e^{\frac{-t}{\tau_{\text{deact}}}},$$

where $I_{\min}$ and $I_{\max}$ describe the minimum and maximum of the voltage dependent activating/deactivating current of the exponential fit. τ_{act} describes the time course of activation and represents the time in milliseconds for the current to reach 1-1/e ($\approx$63%) of I_{max}, respectively τ_{deact} describes the time course of deactivation representing the time for the current to reach 1/e ($\approx$37%) of I_{max}.

4   RESULTS

4.1   KCNQ current

18-27 hours after transfection of CHO cells with eGFP and KCNQ subunit cDNA, voltage clamp experiments were performed. Two pulse protocols were used to investigate KCNQ current characteristics which are shown in **fig. 3**. In a first pulse series (Wang et al. 1998) KCNQ channels were activated from a holding potential of -70 mV. **Fig. 3A** shows slowly activating outward currents in 5 mM $[K^+]_e$ with increasing 10 mV depolarizing voltage increments. Upon hyperpolarisation to -100 mV at the end of the 1 s test pulse, KCNQ currents deactivated faster than they had activated showing an inward tail current. KCNQ deactivation is slow compared to other voltage-gated potassium channels and tail currents are characteristic for KCNQ potassium channels. In the following text this pulse protocol will be called "activation protocol".

A second 3-pulse-protocol (Tatulian et al. 2001) is shown in **fig. 3B** with a constant 1 s depolarisation to +50 mV (P1) before the variable test pulse. The variable 1 s test pulse (P2) between +50 mV and -100 mV is then again followed by a hyperpolarizing pulse (P3) to -100 mV. KCNQ current shows slow activation during P1, slow deactivation during P2 at voltages negative to +20 mV, and inward tail currents at P3. The sweep interval was 7 s. This pulse protocol will be referred to as the "3-pulse-protocol". This 3-pulse-protocol or derivates of it were used for all investigations of KCNQ characteristics except for the analysis of the time course of activation where the activation protocol was used. P1 in the 3-pulse-protocol served as a control for constant KCNQ current. KCNQ current was not stable over time and some experiments showed a greater variation in current amplitude than others as can be seen in **fig. 19** (p.42). Experiments were discarded if they showed a greater then 10% change in current amplitude during successive P1 current traces in order to control for current stability.
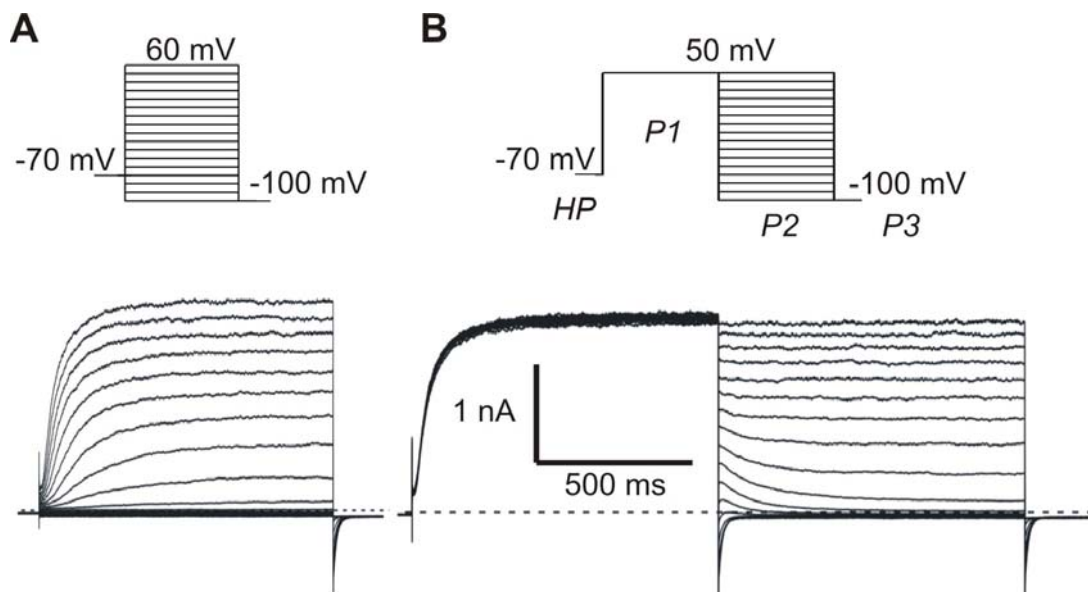
Fig. 3: Current traces of heterologously expressed KCNQ potassium currents
Voltage clamp recording of CHO cells 24 h after transfection with KCNQ2+3 in 5 mM
$[K^+]_e$. **(A)** Activation pulse protocol and respective recorded currents. Cells were kept at a
holding potential of -70 mV followed by a 1s variable test pulse between -100 mV and +60
mV and a 0.5s hyperpolarising pulse to -100 mV before returning to the holding potential.
(B) 3-pulse-protocol and respective recorded currents. Cells were kept at a holding potential
(*HP*) of -70 mV, depolarized for 1s to +50 mV (*P1*), then variably repolarised (*P2*) for 1s
from 50 mV to -100 mV in steps of 10 mV and hyperpolarized to a tail potential (*P3*) of -100
mV for 0.5s before returning to the holding potential (not shown). Sweep intervals were 7 s.

4.2 CHO controls

Non-transfected CHO cells were examined with the same 3-pulse-protocol as KCNQ
transfected cells in order to control for endogenous ionic currents. Where necessary
these native or leak currents were subtracted as specified in section 4.3.3. The same
procedure has been used to control for CHO endogenous currents when investigating
$[K^+]_e$ effects in erg-currents (Sturm et al. 2005). Another way to control for
endogenous current is to specifically block KCNQ currents and examine blocker-
sensitive current. Examination of blocker-sensitive current was not applicable in
these experiments because changes of from low to high $[K^+]_e$ did not allow blocking
in between K^+ changes as channel block was not reversible.

Fig. 4 shows a linear current-voltage relationship measured in 6 non transfected
CHO cells when changing from physiologic to high $[K^+]_e$ and then back to
physiological concentrations. Currents showed an increase in amplitude in high $[K^+]_e$
which was reversible when changing back to low $[K^+]_e$. These endogenous currents
did not show voltage-dependent kinetics.
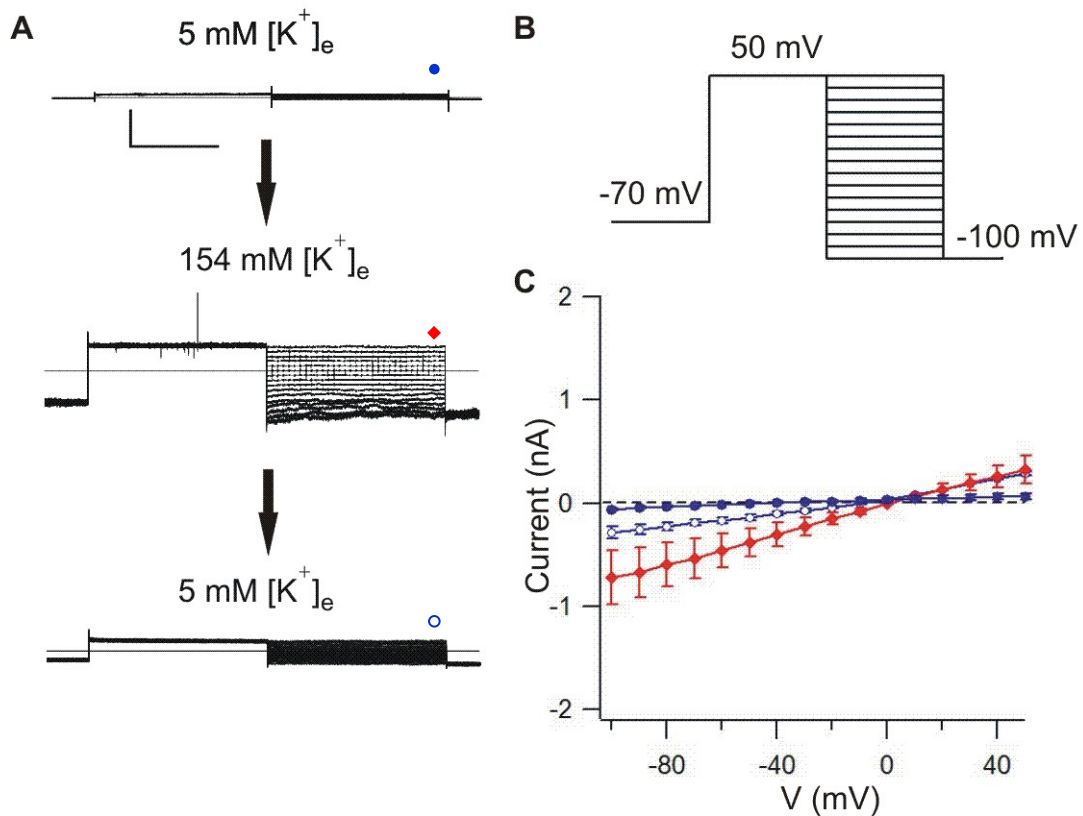
Fig. 4: Endogenous currents in untransfected CHO cells
(A) Cells were kept at a holding potential of -70 mV, depolarized for 1s to 50 mV, then variably repolarized for 1s from 50 mV to -100 mV and hyperpolarized to -100 mV for 0.5s. Endogenous currents are shown in 5 mM extracellular K^+ concentration changing to 156 mM and back to 5 mM. Scale bars represent 500 ms and 1 nA. **(B)** Pulse protocol **(C)** Steady-state currents were measured at the end of the variable pulse and plotted against pipette potential. Error bars represent standard error of the mean; n=6

4.3 Influence of extracellular K^+ concentration on KCNQ currents

The influence of increasing extracellular K^+ from 5 mM to 40 mM and 154 mM has been investigated in CHO cells expressing different KCNQ subunits with respect to voltage dependence of activation, time course of activation and deactivation as well as with respect to conductance changes. The current was examined in CHO cells transfected with KCNQ2, KCNQ3 or KCNQ5 cDNA as well as in cells being co-transfected with KCNQ2+3, KCNQ3+5.

4.3.1 Voltage dependence of activation

Voltage dependence of activation of KCNQ currents was investigated with the 3-pulse-protocol (**fig. 3B**). Exemplary current traces of the different KCNQ subunits in changing $[K^+]_e$ can be seen in **fig. 5**. They show slowly activating potassium outward currents during the first pulse step P1 upon depolarisation to +50 mV. KCNQ2, KCNQ2+3 and KCNQ3+5 current amplitudes during P1 at 5 mM $[K^+]_e$ were 2-4 nA, whereas KCNQ3 and KCNQ5 showed smaller current amplitudes between 0.3 nA and 1.2 nA. Upon repolarisation during P2 all KCNQ subunit currents showed voltage-dependent deactivation. The direction of current changed according to the change in E_K in different $[K^+]_e$. KCNQ2 and KCNQ3 current traces did not show any inactivation of current, whereas KCNQ5 showed recovery of current amplitude in repolarising pulse steps (P2) strongest in low $[K^+]_e$, indicating preceding inactivation (Jensen et al. 2007). Upon hyperpolarisation to -100 mV during a third pulse step P3, inward tail currents can be observed increasing in amplitude with increasing $[K^+]_e$ in accordance with an increase in driving force. The effects were reversed when changing back to the original extracellular ion concentrations at the end of the experiments.

Plotting tail current amplitudes during P3 (**fig. 6** bottom) against the variable prepulse potential during P2 yielded the voltage-dependent activation of current. The resultant sigmoid curve relationship could then be fitted by a Boltzmann function (**fig. 6** left). Characteristic for these sigmoid activation curves are half maximal activation $V_{1/2}$ and slope factor k. $V_{1/2}$ (**fig. 7**) determines the membrane potential in mV of half maximal conductance. k (**fig. 8**) determines the potential shift in mV for a change in normalized conductance from 1/e ($\approx$37%) to 1-1/e ($\approx$63%) which is a measure of the slope of the activation curve - a rise in k corresponds to a decrease in the steepness of the activation curve.

Activation curves for KCNQ2, KCNQ3, KCNQ5, KCNQ2+3 and KCNQ3+5 can be seen in **fig. 6**. All KCNQ channel subunits investigated showed a significant shift in half maximal activation to more negative potentials when increasing extracellular $[K^+]_e$. The activation curve of some but not all KCNQ subunits showed a significant decrease in factor k that is equivalent to an increase in the steepness of the activation curve. A left shift in the activation curve with increasing $[K^+]_e$ was partially or completely reversible when changing back from raised $[K^+]_e$ to the initial low $[K^+]_e$. The change in k was reversible for KCNQ2+3. KCNQ3 did not show reversibility of change in k, whereas KCNQ2 and KCNQ5 showed k to return to values
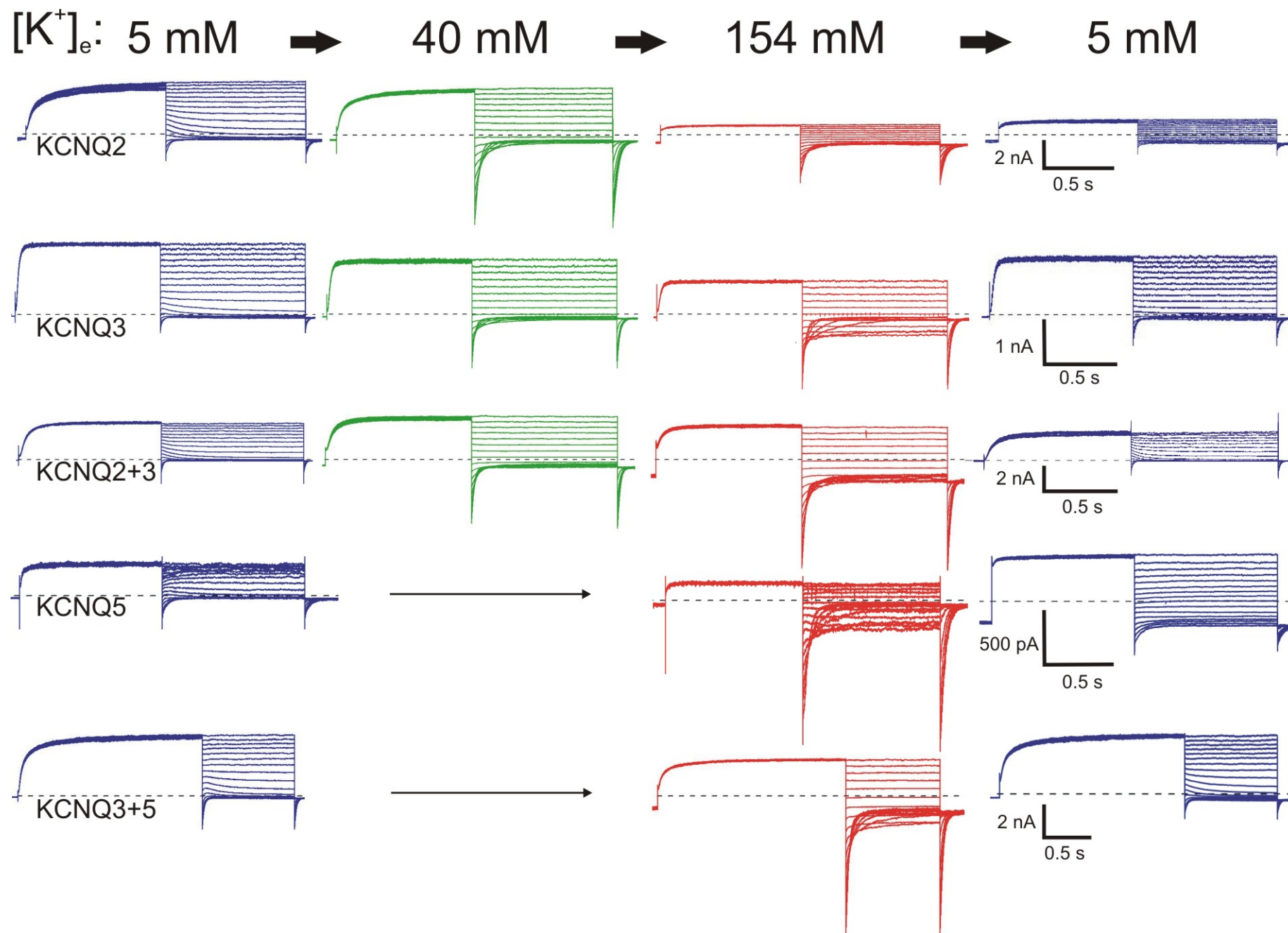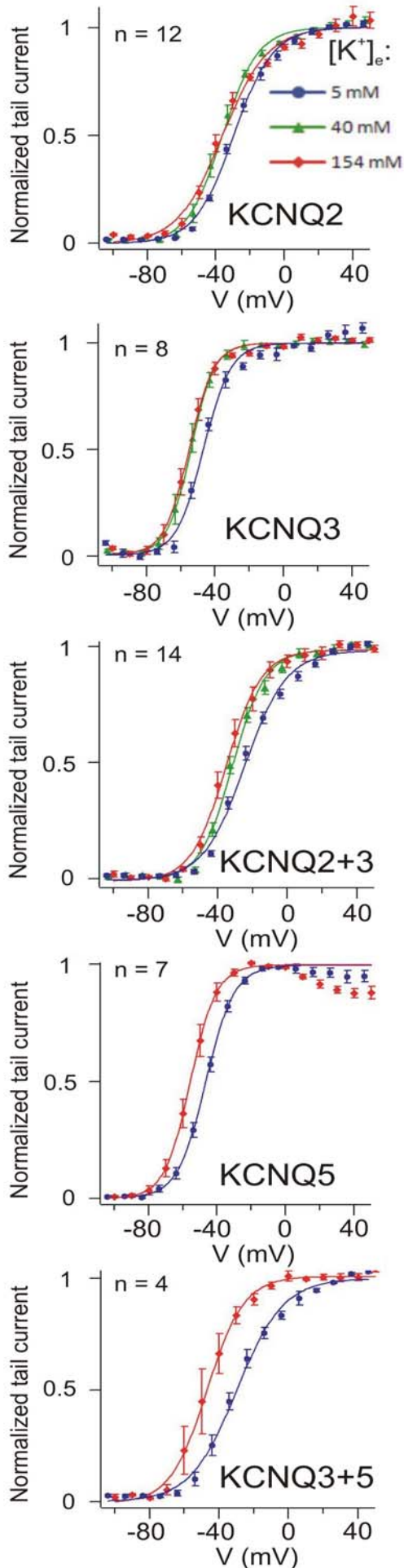
Fig. 5: KCNQ current traces
(*previous page*)
Currents traces were recorded from CHO cells 18-27h after transfection with different KCNQ subunits as indicated. A 3-pulse-protocol was applied in patch-clamp mode. Cells were kept at a holding potential of -70 mV, depolarized for 1s to 50 mV, then variably repolarized for 1s from 50 mV to -100 mV and hyperpolarized to -100 mV for 0.5s. KCNQ currents are shown in 5 mM extracellular K^+ concentration changing to 40 mM, 156 mM and back to 5 mM. The 40 mM step was skipped for KCNQ5 and KCNQ3+5. KCNQ2 shows rundown of current in 154 mM $[K^+]_e$ and back in 5 mM $[K^+]_e$.

Fig. 6: Activation curves determined from tail currents
Curves show voltage-dependent activation of different KCNQ subunit currents. Activation curves were obtained from the tail current amplitude (*see arrow below*) during the tail pulse to -100 mV. Tail amplitude was plotted against membrane potential of the preceding voltage pulse P2 (*left*). Increasing extracellular K^+ concentration from 5 mM (*blue*), to 40 mM (*green*) and 156 mM (*red*) shifted the activation curves of all different KCNQ subunits to more negative potentials.
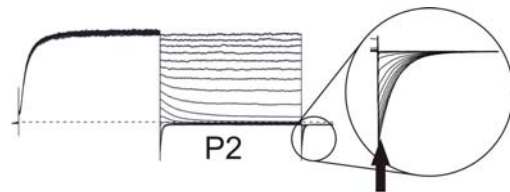
higher than before the increase in $[K^+]_e$. Influences of $[K^+]_e$ on the voltage-dependence of activation are summarized in **fig. 7** and **fig. 8**.

Table 5 shows a summary of the results on page 38.

The membrane potential of half maximal activation of current ($V_{1/2}$) in 5 mM $[K^+]_e$ were for KCNQ2 -29.3±1.5 mV (n=12), for KCNQ3 -47.2±1.1 mV (n=8) , for KCNQ2+3 -26.3±0.9 mV (n=14), for KCNQ5 -46.6±1.2 mV (n=7) and for KCNQ3+5 -29.8±2.3 mV (n=4). After increasing $[K^+]_e$ to 40 mM a significant shift in activation $\Delta V_{1/2}$ could be observed: KCNQ2 -5.9±0.7 mV (p<0.05, n=6), KCNQ3 -6.1±1.8 mV (p<0.05, n=6), KCNQ2+3 -6.4±0.6 mV (p<0.001, n=10); KCNQ5 and KCNQ3+5 were not investigated at 40 mM $[K^+]_e$. Increasing $[K^+]_e$ to 154 mM produced a significant shift $\Delta V_{1/2}$ in activation with respect to 5 mM $[K^+]_e$: KCNQ2 -9.7±0.7 mV (p<0.001, n=11), KCNQ3 -7.0±2.1 mV (p<0.05, n=6), KCNQ 2+3 -10.3±0.7 mV (p<0.0001, n=11), KCNQ5 -9.0±0.9 mV (p<0.01, n=7), KCNQ3+5 -17.2±1.6 mV (p<0.05, n=4). Increasing $[K^+]_e$ to 80 mM $[K^+]_e$ was only carried out for KCNQ2 and showed a shift $\Delta V_{1/2}$ of -9.7±1.0 mV (p<0.01, n=4).
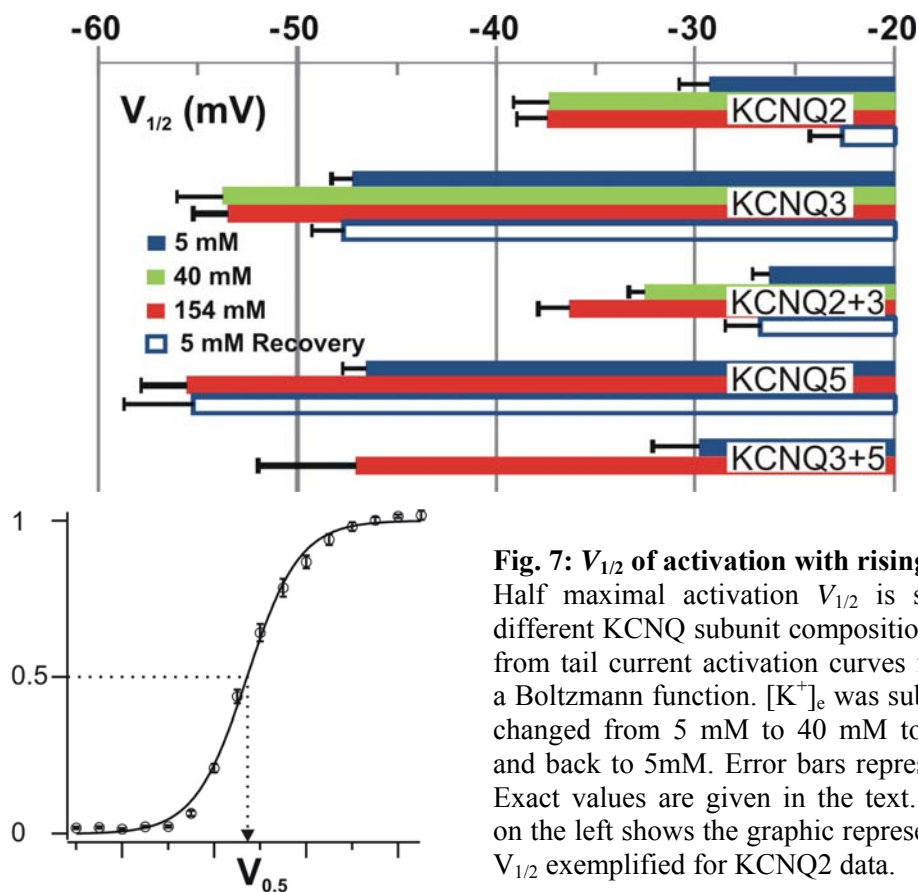
Fig. 7: $V_{1/2}$ of activation with rising $[K^+]_e$
Half maximal activation $V_{1/2}$ is shown for different KCNQ subunit compositions derived from tail current activation curves fitted with a Boltzmann function. $[K^+]_e$ was subsequently changed from 5 mM to 40 mM to 154 mM and back to 5mM. Error bars represent SEM. Exact values are given in the text. The inset on the left shows the graphic representation of $V_{1/2}$ exemplified for KCNQ2 data.
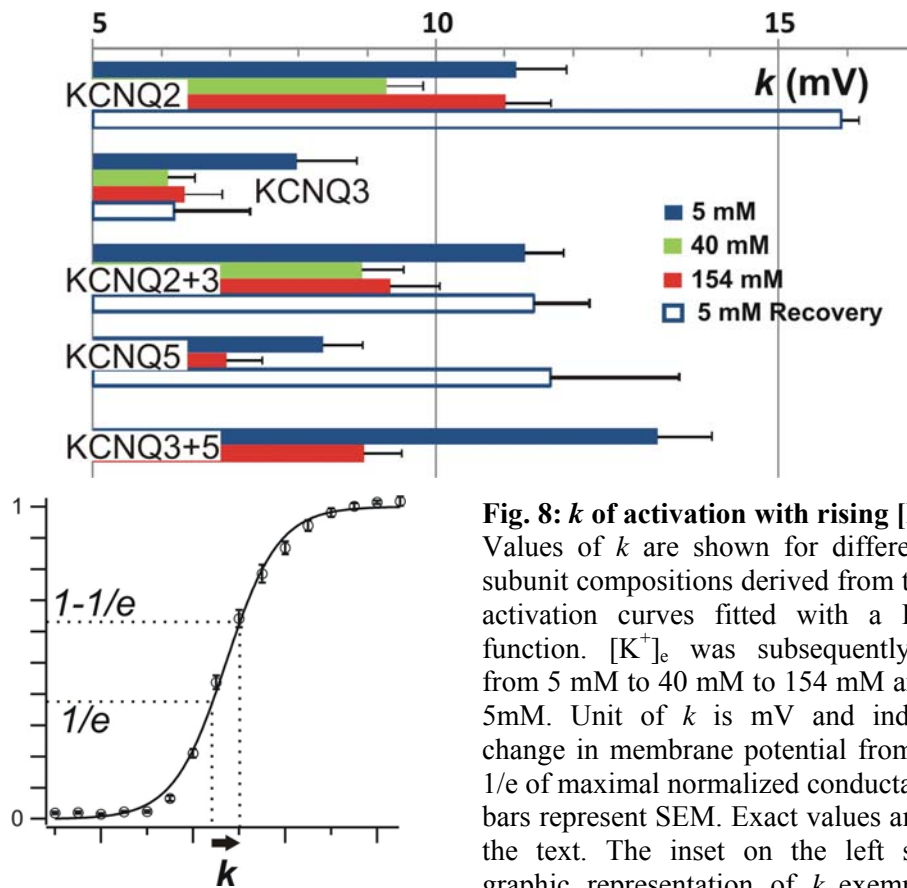
Fig. 8: k of activation with rising $[K^+]_e$
Values of k are shown for different KCNQ subunit compositions derived from tail current activation curves fitted with a Boltzmann function. $[K^+]_e$ was subsequently changed from 5 mM to 40 mM to 154 mM and back to 5mM. Unit of k is mV and indicates the change in membrane potential from 1/e to 1-1/e of maximal normalized conductance. Error bars represent SEM. Exact values are given in the text. The inset on the left shows the graphic representation of k exemplified for KCNQ2 data.

Slope factor k in 5 mM $[K^+]_e$ was as follows: for KCNQ2 11.2±0.7 mV (n=12), for KCNQ3 8.0±0.9 mV (n=8), for KCNQ2+3 11.3±0.6 mV (n=14), for KCNQ5 8.4±0.6 mV (n=7) and for KCNQ3+5 13.2±0.8 mV (n=4). Increasing $[K^+]_e$ to 40 mM resulted in a significant decrease in k, increasing the steepness of the activation curve. Change in k in 40 mM $[K^+]_e$ compared to 5 mM $[K^+]_e$: KCNQ3 -1.9±0.6 mV (p<0.05, n=6); KCNQ2+3 -2.4±0.4 mV (p<0.001, n=10). A change in k for KCNQ2 was not significant (-1.9±0.8 mV; p=0.38, n=6); KCNQ5 and KCNQ3+5 were not investigated at 40 mM $[K^+]_e$. Increasing $[K^+]_e$ to 154 mM produced a significant decrease in k compared to 5 mM $[K^+]_e$. Change in k in 154 mM $[K^+]_e$ compared to 5 mM $[K^+]$: KCNQ2+3 -1.9±0.5 mV (p<0.05, n=11); KCNQ5 -1.4±0.6 mV (p<0.05, n=7) and KCNQ3+5 -4.3±1.0 mV (p<0.05, n=4). Changes in k were not significant for KCNQ2 -0.2±1.0 mV (p=0.37, n=11) and KCNQ3 -1.6±1.3 mV (p=0.42, n=6). Increasing $[K^+]_e$ to 80 mM was only done for KCNQ2 and showed no significant change in k (-1.1±1.2 mV, p=0.36, n=4).

Statistical significance for $V_{1/2}$ and k changes in higher $[K^+]_e$ was tested for with a one tail paired t-test as a left shift and an increase in the steepness of the activation curves were found at the node of Ranvier (Schwarz et al. 2006). The effects seen when increasing $[K^+]_e$ could be partly or completely reversed after changing the extracellular bath solution back to the initial concentration of 5 mM $[K^+]_e$.

$V_{1/2}$-recovery values after this change differed from the initial $V_{1/2}$ at the start of experiments by the following amount: KCNQ2 4.5±0.3 mV (p=0.007); KCNQ3 -0.6±0.8 mV (p=0.24); KCNQ2+3 -1.7±1.0 mV (p=0.23) and KCNQ5 -5.4±1.0 mV (p=0.08). k recovery values changing back from high $[K^+]_e$ to 5 mM differed by: KCNQ2 4.7±0.4 mV (p=0.03); KCNQ3 -1.8±0.9 mV (p=0.26); KCNQ2+3 -1.1±0.6 mV (p=0.11) and KCNQ5 2.5±0.7 mV (p=0.08).

Difficulties appeared when fitting sigmoid curves for voltage dependence of KCNQ5 activation as this channel shows slow inactivation properties (Jensen et al. 2007). Sigmoid curve fitting was therefore only done between -100 mV and 0 mV as channel conductance starts to decrease again at potentials positive to 0 mV due to inactivation. $V_{1/2}$ and k values for KCNQ5 could then be determined but might not solely represent voltage dependence of activation but rather a mixture of activation and inactivation.

In summary tail current analysis of voltage dependence of KCNQ activation showed a significant shift to more negative potentials with a significant steepening of voltage dependence of activation with increases in $[K^+]_e$.

4.3.2 Time course of KCNQ2+3 activation and deactivation

The time course of activation and deactivation of KCNQ current is voltage-dependent. KCNQ currents activate more quickly the higher the depolarisation potential. But does a change in the extracellular K^+ concentration influence activation or deactivation kinetics? To answer this question activation and deactivation time constants were determined for different pipette potentials in changing $[K^+]_e$. Pulse protocols used were derivatives of the activation protocol and deactivating 3-pulse-protocol.

Activation of KCNQ2+3 current was initiated from a holding potential of -70 mV by depolarisation of the membrane to a variable potential of -40 mV to +60 mV for 1 s, where time courses could be exponentially fitted and compared in different extracellular potassium concentrations. The exponential time course of activation at different depolarising potentials can be seen in current traces displayed in **fig. 9**.

In 5 mM $[K^+]_e$ one can see that the outward current activates more quickly as the depolarisation potential is increased. In 154 mM $[K^+]_e$ depolarisation to negative membrane   potentials   now   starts   to   activate   a   KCNQ
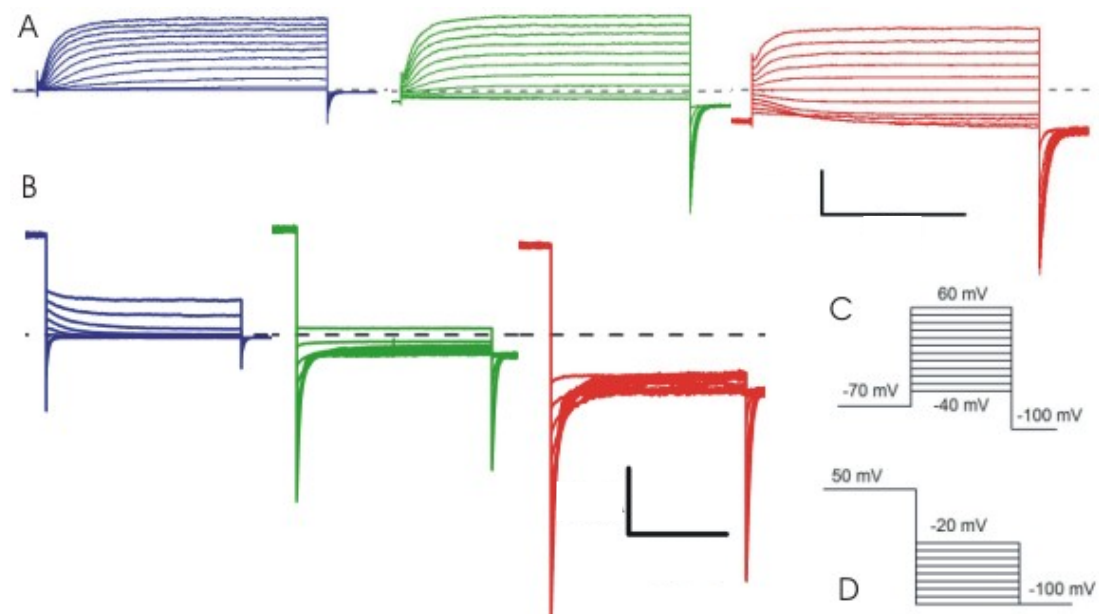
Fig. 9: Current traces of KCNQ2+3 activation and deactivation in changing $[K^+]_e$
(A) Activation of KCNQ2+3 current was initiated from a holding potential of -70 mV by depolarisation of the membrane to a variable potential of -40 mV to +60 mV for 1s. **(B)** After full activation by a 1s depolarising pulse to +50 mV a variable repolarisation to membrane potentials between -20 mV and -100 mV shows deactivation of KCNQ2+3 current. $[K^+]_e$ was subsequently changed from 5 mM (*blue*) to 40 mM (*green*) and 154 mM (*red*). Current traces showed an increase in non-specific leak current in high $[K^+]_e$. Scale bars represent 2 nA and 0.5 s. Pulse protocol of activation **(C)** and deactivation **(D)**.

inward current. The current reversed direction near 0 mV, the calculated E_K in 154 mM $[K^+]_e$. Fitting the time course of activation with a single exponential function (Suh and Hille 2007) resulted in a decrease in τ_{act} with each further depolarisation. T_{act} is plotted against test pulse potential in **fig. 10**. Concrete values of τ_{act} are given in **table 4** as mean and SEM for 6 cells expressing KCNQ2+3 in changing $[K^+]_e$ from 5 to 40 and 154 mM. When comparing τ_{act} at a higher $[K^+]_e$ with the initial 5 mM $[K^+]_e$, the acceleration of current activation with the higher $[K^+]_e$ at depolarising potentials between -40 mV and +10 mV is significant at both 40 and 154 mM $[K^+]_e$ levels. This accelerating effect was only partially reversible when changing $[K^+]_e$ back from 154 mM to 5 mM (recovery values in **table 4**).

The time course of deactivation in changing $[K^+]_e$ was investigated in current traces that could be exponentially fitted from the 3-pulse protocol used for the analysis of the voltage dependence of activation. Full activation of current was achieved by a 1s depolarising pulse to +50 mV. A following variable repolarisation to potentials between -20 mV and -100 mV showed deactivation of the KCNQ2+3 current (**fig. 9**). The time course of voltage-dependent deactivation was fitted with an exponential function yielding the time constant τ_{deact} (see also section 3.3.7). A significant change in τ_{deact} when going to a higher $[K^+]_e$ could be observed upon repolarisation to potentials positive to -40 mV and negative to -80 mV. KCNQ2+3 deactivation
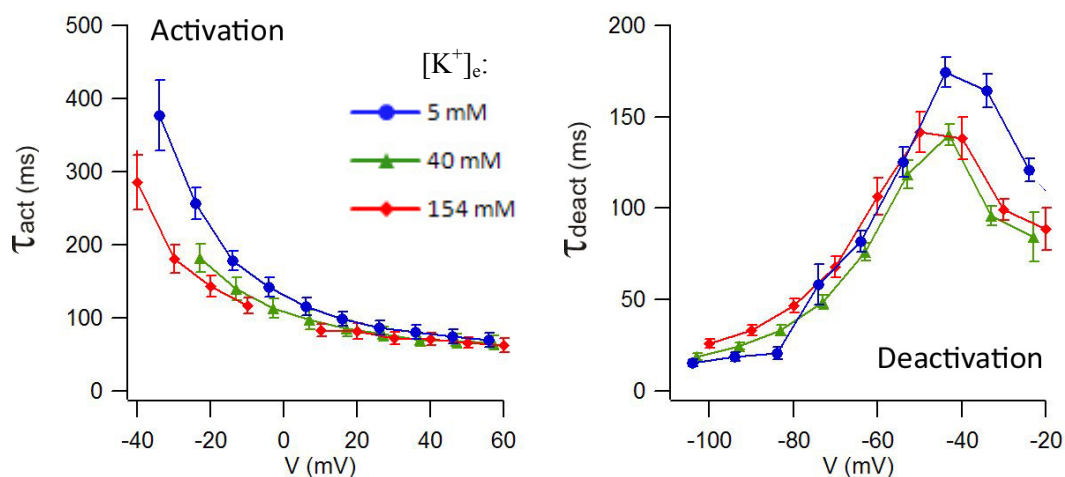
Fig. 10: Voltage-dependent time course of activation and deactivation in rising $[K^+]_e$
Time constants of KCNQ2+3 activation τ_{act} and deactivation τ_{deact} were plotted against membrane potential. $[K^+]_e$ was changed from 5 mM to 40 mM and 154 mM. Determining time constants of activation near E_K was not practical and is therefore not shown. V (mV) denotes membrane potential. The membrane potential plotted was corrected for liquid junction potentials offline changing in different $[K^+]_e$. (n=6)

shows acceleration above -40 mV and slowing at more negative potentials than -80 mV when increasing $[K^+]_e$ (**fig. 10** and **table 4**).

Deactivation by repolarising the membrane to potentials of between -80 mV and -40 mV did not show any significant change in τ_{deact} in higher $[K^+]_e$. Effects on deactivation showed reversibility only to voltages negative to -80 mV when changing back from high to the initial 5 mM $[K^+]_e$. Liquid junction potential errors were not taken into account when comparing time courses of activation and deactivation (as in **table 4**) and when testing for statistical significance as the correction of the pipette potentials was performed offline. Graphical presentation in **fig. 10** was corrected for liquid junction potentials by offline correction and the membrane potential was plotted on the x-axis. Liquid junction potential errors are discussed in section 5.1.7.

In summary increasing $[K^+]_e$ showed acceleration of activation and deactivation to membrane potentials above -40 mV whereas it showed slowing of deactivation to potentials below -80 mV.

Table 4: Voltage-dependent time constants of KCNQ2+3 activation and deactivation in changing $[K^+]_e$

Time constants of activation were determined by depolarisation from -70 mV holding potential to a variable membrane potential and are given as mean and SEM in seconds. **(*)** Determination of activation time constants near E_K was not possible and was therefore omitted. Voltage-dependent time constants of deactivation were determined by repolarisation from +50 mV to a variable membrane potential. P-values for time constants in 40 mM, 154 mM and recovery 5 mM $[K^+]_e$ denote statistical testing with respect to time constants in initial 5 mM $[K^+]_e$. V(mV) denotes pipette potential. Statistical significance is marked in orange.

Activation τ_{act} [s] (n=6)											
V (mV)	5 mM $[K^+]_e$		40 mM $[K^+]_e$			154 mM $[K^+]_e$			5 mM $[K^+]_e$ Recovery		
	mean	SEM	mean	SEM	p=	mean	SEM	p=	mean	SEM	p=
-40	0.632	0.137	*	*	*	0.286	0.037	0.042	0.349	0.143	0.315
-30	0.377	0.048	*	*	*	0.181	0.019	0.001	0.269	0.042	0.166
-20	0.257	0.022	0.182	0.019	0.002	0.143	0.014	0.000	0.196	0.016	0.124
-10	0.179	0.013	0.140	0.016	0.006	0.116	0.011	0.000	0.151	0.006	0.173
0	0.142	0.013	0.113	0.013	0.011	*	*	*	0.129	0.008	0.235
10	0.115	0.012	0.098	0.013	0.018	0.084	0.008	0.005	0.116	0.005	0.536
20	0.098	0.010	0.085	0.011	0.061	0.082	0.011	0.001	0.106	0.010	0.671
30	0.087	0.010	0.078	0.010	0.059	0.073	0.009	0.009	0.087	0.004	0.590
40	0.081	0.010	0.069	0.008	0.059	0.071	0.009	0.049	0.091	0.008	0.944
50	0.075	0.010	0.069	0.010	0.086	0.066	0.007	0.284	0.078	0.007	0.714
60	0.070	0.009	0.066	0.009	0.230	0.063	0.009	0.218	0.087	0.008	0.590
Deactivation τ_{deact} [s] (n=6)											
-20	0.121	0.006	0.084	0.014	0.011	0.089	0.012	0.110	0.093	0.011	0.217
-30	0.164	0.009	0.096	0.005	0.001	0.099	0.006	0.002	0.097	0.001	0.045
-40	0.174	0.008	0.140	0.006	0.000	0.138	0.011	0.003	0.108	0.005	0.019
-50	0.125	0.008	0.119	0.008	0.299	0.142	0.011	0.272	0.077	0.006	0.037
-60	0.082	0.006	0.076	0.005	0.140	0.106	0.010	0.083	0.067	0.011	0.105
-70	0.058	0.011	0.049	0.004	0.283	0.068	0.006	0.461	0.030	0.011	0.046
-80	0.021	0.003	0.033	0.003	0.016	0.047	0.004	0.007	0.031	0.008	0.051
-90	0.019	0.002	0.025	0.002	0.010	0.033	0.003	0.005	0.022	0.004	0.318
-100	0.016	0.002	0.019	0.002	0.032	0.026	0.002	0.004	0.016	0.002	0.430

4.3.3 Voltage-dependent whole-cell conductance

The voltage dependence of whole-cell conductance was obtained by determining current amplitudes at the end of 1 s voltage pulses between -100 mV and +50 mV in 10 mV increment. The current traces analysed were the same as those used for determining voltage dependence of activation from tail currents. An example of a family of current traces can be seen in the inset of **fig. 11A**. The current recorded at the end of the variable voltage pulse (P2) was converted into whole-cell conductance and compared with changing $[K^+]_e$.
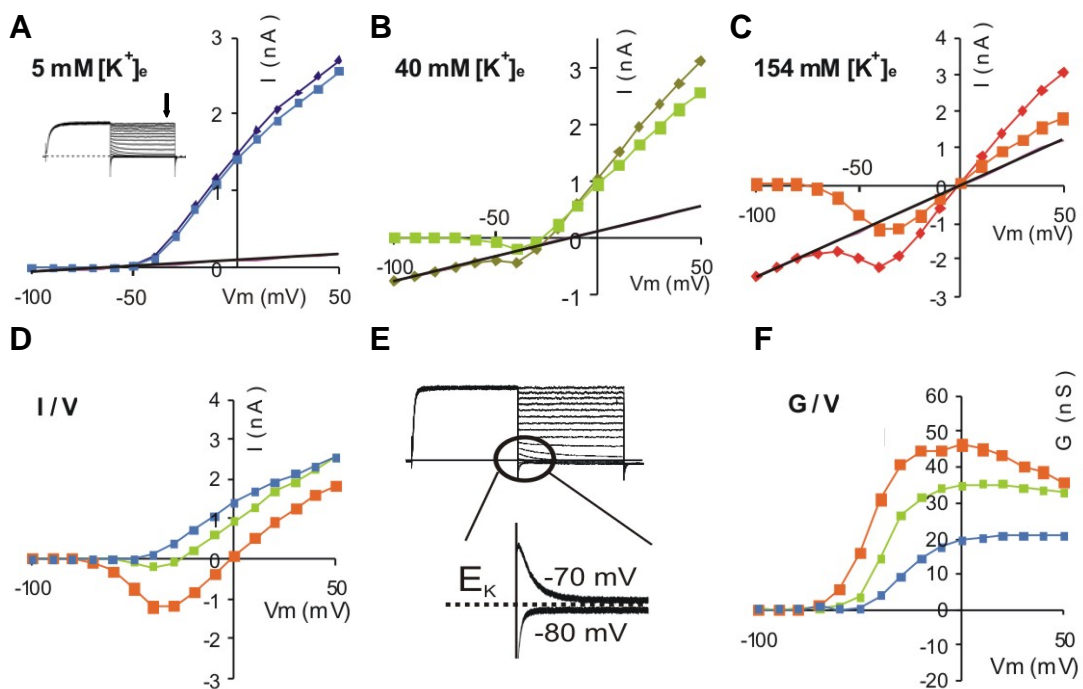
Fig. 11: Conversion of current voltage data to conductance curves
(A)-(C) Example of KCNQ current voltage relationships before and after correction for non KCNQ specific current at different $[K^+]_e$ for one cell. Current was recorded at the end of a 1s pulse to a variable membrane potential between -100 and +50 mV (*see arraow in inset A*). The linear regression line of non KCNQ specific current is shown in black. **(D)** Current-voltage relationship at 5, 40 and 154 mM $[K^+]_e$ corrected for non-specific current. **(E)** Estimation of E_K in 5 mM $[K^+]_e$ for conversion of current-voltage to conductance-voltage data. The circled area is enlarged and shows the reversal of potassium current relaxation direction from outward to inward. **(F)** shows the sigmoid shaped voltage-dependent conductance in different $[K^+]_e$.

Current recordings from CHO controls (in section 4.2) showed a non KCNQ specific leak current. This linear leak current (*black lines* in **fig. 11A-C**) was subtracted before converting KCNQ current into conductance.

Leak current was subtracted for each recorded data point respective to its membrane potential and $[K^+]_e$. Potential-dependent non-specific leak current was determined by

a linear regression between the 3 most negative membrane potentials with KCNQ specific current still deactivated. After correction for non-specific leak current KCNQ current-voltage relationships were obtained for different extracellular potassium concentrations (**fig. 11D**).

Conversion of these leak-corrected steady-state KCNQ current amplitudes into conductance values using the calculated E_K did not yield a sigmoid conductance-voltage relationship (Data not shown). These curves showed large deviations around E_K and no levelling off at positive and negative extremes of membrane voltage. However, a sigmoid conductance curve was expected from the KCNQ behaviour as described in the literature and earlier activation analysis from tail currents (section **4.3.1**). Estimation of E_K from looking at the reversal from outward to inward potassium current is shown in **fig. 11E**. These empirical estimates of E_K were more positive than E_K calculated from the intracellular and extracellular concentrations of K^+ ions. Using these optical estimates of E_K in the conversion of current to conductance values now resulted in sigmoid conductance-voltage relationships (**fig.11F**).
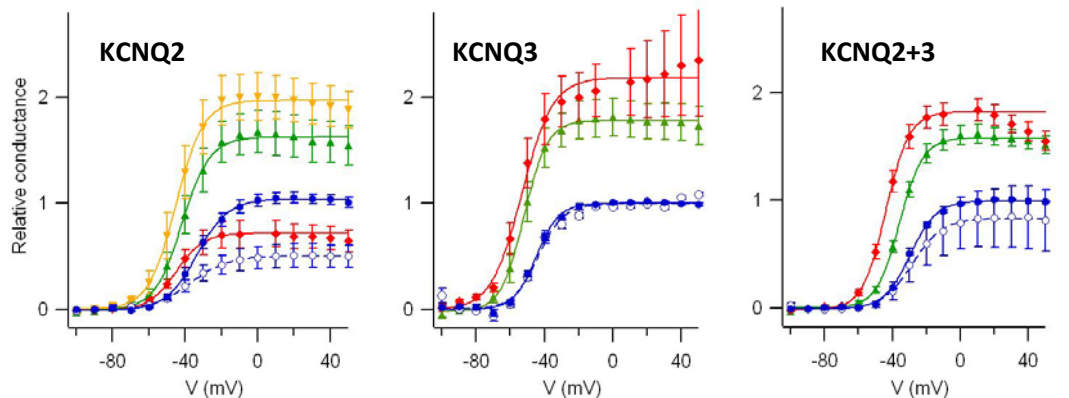
Fig. 12: Increase in conductance with rising $[K^+]_e$
Conductance of different KCNQ subunit compositions relative to maximal conductance at 5 mM $[K^+]_e$ is plotted against membrane potential. Conductance was calculated by $G=I/(V_{mem}-E_K)$ as described in the text and fitted by sigmoid regression using a Boltzmann function. $[K^+]_e$ was subsequently changed from 5 to 40 to 154 mM and back to 5 mM during the experiment. 80 mM was only tested for KCNQ2. For colour coding see the inset on the right.

The values for E_K observed from the current traces used for current-conductance conversions **(fig. 11E)** were: -75.9±2.4 mV at 5 mM $[K^+]_e$, -27.3±0.5 mV at 40 mM $[K^+]_e$, -22.2±3.8 mV at 80 mM $[K^+]_e$, -0.3±0.8 mV at 154 mM $[K^+]_e$ and -63.0±5.6 mV when changing back to 5 mM $[K^+]_e$. Whereas E_K values calculated from Nernst's equation at 25 °C were: -88 mV at 5 mM $[K^+]_e$, -35 mV at 40 mM $[K^+]_e$, -17 mV at 80 mM $[K^+]_e$ and 0.3 mV at 154 mM. Possible explanations for these difference in E_K between calculated and observed values of E_K are part of the discussion.

Sigmoid conductance curves were obtained after correction for leak currents and potassium reversal potential. These conductance curves were then fitted by a sigmoid Boltzmann function **(fig. 12)** and maximum conductance values from these fits could be compared at different $[K^+]_e$ for KCNQ2, KCNQ3 and KCNQ2+3 **(fig. 13)**.
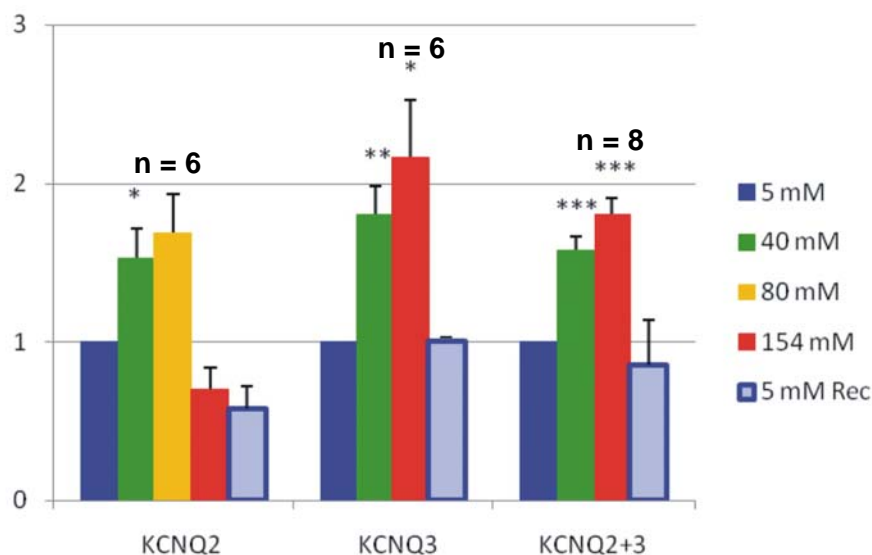
Fig. 13: Changes in maximal whole-cell conductance with rising $[K^+]_e$
Comparison of conductance determined from the maximum of the sigmoid curve fit to G/V-curves for KCNQ2, KCNQ3 and KCNQ2+3 currents. Maximal conductance is compared at different $[K^+]_e$ and colour coded as shown on the right of the graph. Maximal conductance was normalized to maximal conductance at initial 5 mM $[K^+]_e$. Error bars represent SEM. Exact values are given in the text. A concentration of 80 mM $[K^+]_e$ was only done for KCNQ2. These experiments were of longer duration than for KCNQ3 and KCNQ2+3 and run-down effects possibly explaining the decreased conductance at high $[K^+]_e$ for KVNQ2 will be discussed later. Statistical significant change with respect to the initial 5 mM $[K^+]_e$ was tested by a paired t-test (* $p<0.05$, ** $p<0.01$, *** $p<0.001$).

Maximal whole-cell conductance at 5 mM $[K^+]_e$ was: KCNQ2 26.1±3.7 nS (n=6), KCNQ3 6.3±1.2 nS (n=6) and KCNQ2+3 27.3±6.7 nS (n=8). Conductance of KCNQ increased after rising the $[K^+]_e$ in the bath to 40 mM to: KCNQ2 152.9%±18.9% (p<0.05); KCNQ3 180.8%±17.4% (p<0.01); KCNQ2+3 158.0%±8.2% (p<0.05). A

further increase to 80 mM $[K^+]_e$ was only done for cells expressing KCNQ2. Conductance increased in comparison to 5 mM $[K^+]_e$ to 168.9%±23.9% (p=0.10). A further rise in $[K^+]_e$ to 154 mM increased conductance for KCNQ3 and KCNQ2+3 but not for KCNQ2. KCNQ2 showed rundown of current both in 154 mM $[K^+]_e$ and changing back to 5 mM $[K^+]_e$ after the additional increase to 80 mM $[K^+]_e$ which was not done for KCNQ3 and KCNQ2+3.The relative conductance in 154 mM $[K^+]_e$ with respect to the initial 5 mM $[K^+]_e$ was: KCNQ2 70.6%±13.5% (p=0.06); KCNQ3 216.8%±35.9% (p<0.05); KCNQ2+3 180.7%±10.4% (p<0.001).

The increase in conductance in high $[K^+]_e$ was reversible after lowering $[K^+]_e$ at the end of the experiment to the initial 5 mM $[K^+]_e$. The end values of whole-cell conductance obtained after changing back to 5 mM $[K^+]_e$ in relation to initial conductance at 5 mM $[K^+]_e$, did not differ significantly: KCNQ2 57.5%±14.5% (p=0.06); KCNQ3 100.0%±0.1% (p=0.38); KCNQ2+3 85.3%±28.9% (p=0.70).

4.4 Methodological aspects of KCNQ activation analysis

4.4.1 Comparing the analysis of tail currents to that of steady-state currents

The voltage dependence of activation has been compared in different $[K^+]_e$ by analysis of tail currents in chapter **4.3.1** . The maximum amplitude of conductance in different $[K^+]_e$ has been investigated in the previous chapter **4.3.3**. In the latter investigation, the conductance at the end of the variable voltage pulse was calculated and fitted with a Boltzmann function. The voltage dependence of this conduction is also a measure of channel activation obtained by a different approach as in tail current analysis. Both types of analysis are commonly used by different authors. In this chapter, the results of investigating the voltage dependence of KCNQ activation and its changes with a rising $[K^+]_e$ obtained by these two different methods will be compared in order to show if both approaches lead to the same results.

Tail currents, as used for examination of KCNQ activation in **4.3.1**, reflect conductance at the preceding variable voltage pulse (P2). One would expect that half maximal activation $V_{1/2}$ and slope factor k found by tail current analysis mirrors steady-state conductance at the end of the variable voltage pulse (P2). **Fig. 14** shows voltage-dependent current at the end of the variable voltage pulse on the left for different KCNQ subunits and different $[K^+]_e$. This current was converted into

conductance, normalized and fitted with a Boltzmann function. The same method was used for the calculation of voltage-dependent conductance from currents as in as described the previous chapter **4.3.3**. Characteristics of the voltage dependence of conductance and therewith current activation could then be compared to the results obtained from tail current analysis seen on the right.
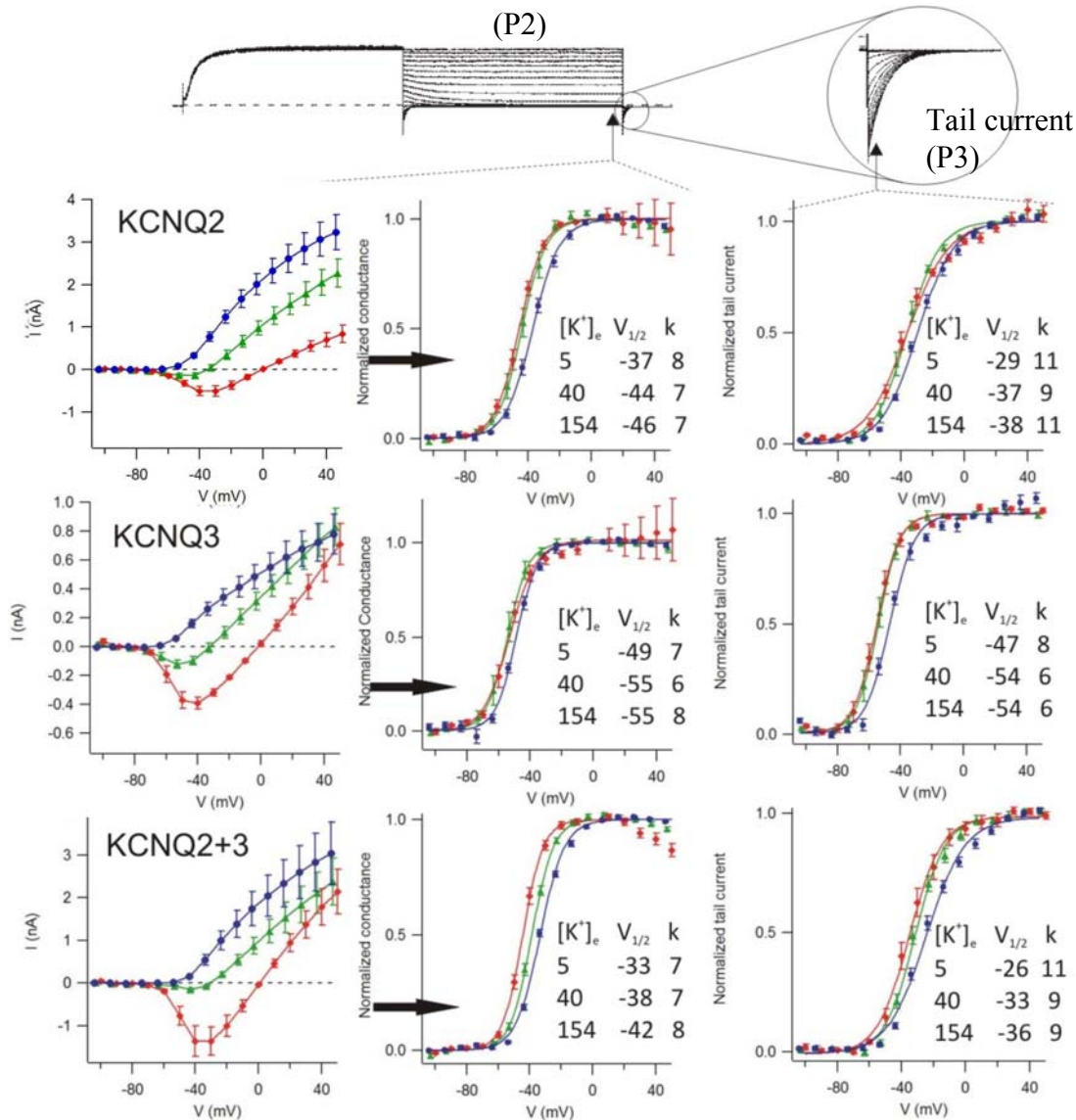
Fig. 14: Comparison of KCNQ voltage-dependent activation from steady-state current and tail current analyses
Typical KCNQ current traces in 5 mM $[K^+]_e$ are shown while applying the 3-pulse- protocol at the top. Tail currents during a voltage pulse to -100 mV (P3) are depicted enlarged at the top right. Voltage-dependent currents are plotted on the left in changing $[K^+]_e$ (*blue* 5 mM, *green* 40 mM, *red* 154 mM) for the different KCNQ subunits. These voltage-dependent currents were converted into conductance, normalized to its maximum and fit by a Boltzmann function in the middle coloumn. Voltage dependence of KCNQ activation determined from tail current analysis is shown on the right. Membrane potential of half maximal activation $V_{1/2}$ and slope factor k determined from the Boltzmann fits to the data are given in mV for the different $[K^+]_e$ in mM. Voltages were corrected for liquid junction potential errors.
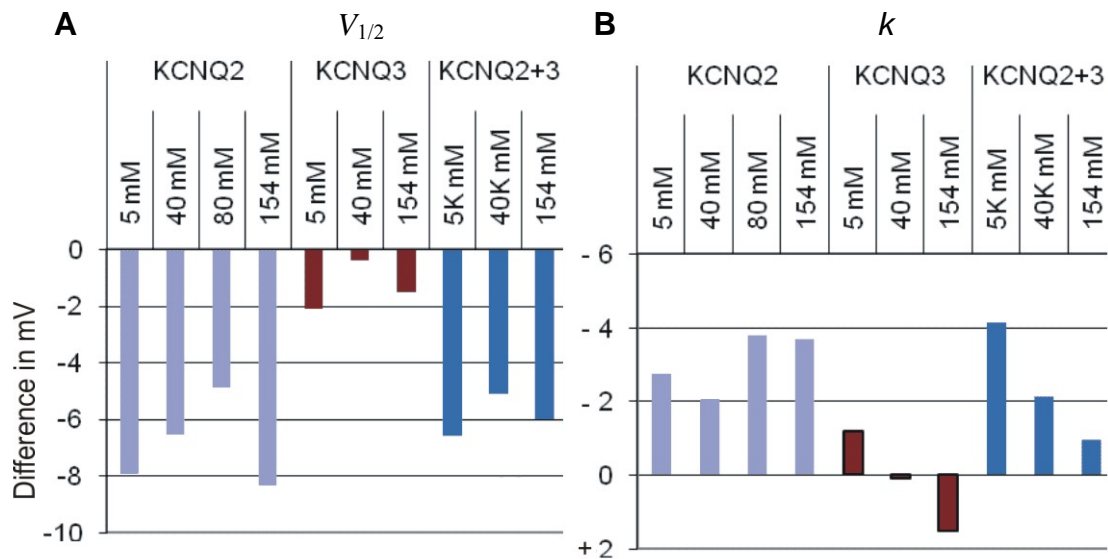
Fig. 15: Comparison of the activation curves obtained from the two different modes of KCNQ analysis: results of steady-state current analysis vs. tail current analysis
Activation curves from steady-state currents were at more negative potentials and steeper than activation curves obtained from tail currents. **A** shows the difference in absolute $V_{1/2}$ for different KCNQ subunits and different $[K^+]_e$ when comparing the analysis of steady-state currents with respect to that of tail-currents. **B** compares the steepness of the activation curves between steady-state current analysis and tail-current analysis of the same measurements. The smaller the value of k, the steeper is the sigmoid activation curve.

In general, steady-state current activation curves on the left in **fig. 14** are steeper and in a more negative voltage range when compared to activation curves determined from tail currents on the right.

Values of $V_{1/2}$ and k obtained from steady-state current for the different KCNQ subunits and different extracellular K^+ concentrations showed $V_{1/2}$ to be 4.9±0.9 mV (p<0.001) more negative and k to be 1.9±0.6 mV (p<0.01) smaller than those obtained from tail currents in the same reading.

There was a discrepancy in this observation when regarding different KCNQ subunit compositions. **Fig. 15** shows the difference in $V_{1/2}$ and k comparing the two methods of analysis. The discrepancy is slightly greater in KCNQ2 than KCNQ2+3 (*blue and purple*) and only small in KCNQ3 analysis (*red*) for both $V_{1/2}$ and k. A substantial difference between KCNQ2 and KCNQ2+3 on the one hand compared to KCNQ3 on the other is the overall current amplitude as can be seen in current voltage plots in **fig. 14**. The average current amplitudes at +50 mV in 5 mM $[K^+]_e$ were approximately 3 nA for KCNQ2 and KCNQ2+3, whereas the KCNQ3 current was only around 0.7 nA. Respectively the maximal whole cell conductance at 5 mM $[K^+]_e$

was between 26 nS and 28 nS for KCNQ2 and KCNQ2+3, whereas KCNQ3 showed a conductance of only 6 nS as described in chapter **4.3.3**.

The effect of increasing $[K^+]_e$ on KCNQ activation was then compared between the two methods of analysis of voltage dependence of activation. The negative shift in $V_{1/2}$ was significant in both types of data analysis. The shift in $V_{1/2}$ obtained from the examination of steady-state conductance was found to be smaller by 16.1±7.3% (p<0.05) than the voltage shift found analysing tail currents. A sub-analysis of the amplitude of shift in $V_{1/2}$ for different KCNQ subunits can be found in **fig. 16**. Here the negative shift in the voltage dependence of activation in increasing $[K^+]_e$ found by steady-state conductance analysis is given as a percentage of the negative shift in $V_{1/2}$ found in the analysis of tail currents. Comparing a change in the steepness of voltage-dependent activation in rising $[K^+]_e$ did not show to be significant when analysing steady-state conductance. An increase in the steepness of voltage-dependent activation in rising $[K^+]_e$ could be observed analysing tail currents (section **4.3.1**) when increasing $[K^+]_e$ from 5 mM to 40 mM.

In summary, a significant left shift in the voltage dependence of activation $\Delta V_{1/2}$ with increasing $[K^+]_e$ levels found by tail current analysis can be confirmed when analysing steady-state current, whereas an increase in the slope of activation curve cannot. The absolute appearance of the activation curve is significantly steeper and at significantly more negative potentials when analysing steady-state currents than with the analysis of tail current.
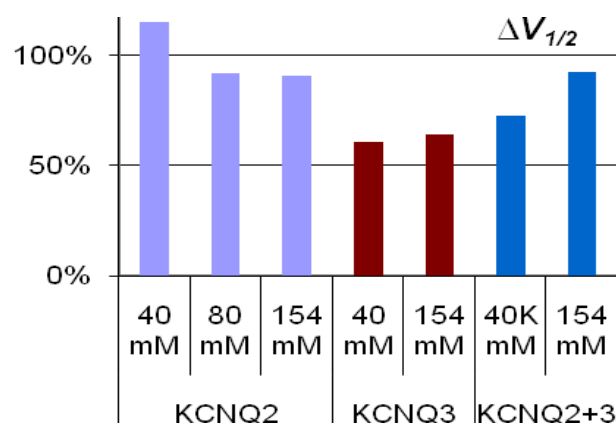
Fig. 16: Comparison of $V_{1/2}$ change in rising $[K^+]_e$ between steady-state current and tail current analysis
One effect of increasing $[K^+]_e$ on KCNQ activation was a shift of $V_{1/2}$ to more negative potentials. The figure compares the amount of shift in $V_{1/2}$ found when analysing steady-state currents as a percentage of the shift found when analysing tail currents.

Table 5: Summary of Data
The table shows a summary of the data obtained for $V_{1/2}$ and k as well as its changes in rising $[K^+]_e$ and its recovery control at the end of the experiment for KCNQ2, KCNQ3 and KCNQ2+3.

Channel	Analysis	$[K^+]_e$ (mM)	$\Delta V_{1/2}$ (mV) Δ	SEM	p	$V_{1/2}$ (mV) Mean	SEM	n	k (mV) Mean	SEM	Δk (mV) Δ	SEM	p
KCNQ2	Tail currents	5				-29.3	± 1.5	12	11.2	± 0.7			
		40	-5.9	± 0.7	0.01	-37.4	± 1.8	6	9.3	± 0.5	-1.9	± 0.8	0.38
		80	-9.7	± 1.0	0.01	-43.2	± 2.4	4	10.1	± 0.5	-1.1	± 1.2	0.36
		154	-9.7	± 0.7	0.01	-37.5	± 1.5	11	11.0	± 0.7	-0.2	± 1.0	0.37
		5 Rec	4.5	± 0.3	0.01	-22.6	± 1.6	2	15.9	± 0.3	4.7	± 0.4	0.03
	Steady state current	5				-37.2	± 1.3	10	8.4	± 0.3			
		40	-6.8	± 0.5	0.01	-43.9	± 2.0	6	7.2	± 0.9	-1.2	± 1.0	0.59
		80	-8.9	± 0.9	0.01	-48.1	± 3.3	3	6.3	± 0.6	-2.1	± 0.8	0.19
		154	-8.8	± 0.7	0.01	-45.9	± 1.4	9	7.3	± 0.3	-1.1	± 0.5	0.05
		5 Rec	-0.9	± 0.6	0.19	-37.5	± 1.8	6	10.2	± 1.6	1.8	± 1.6	0.40
KCNQ3	Tail currents	5				-47.2	± 1.1	8	8.0	± 0.9			
		40	-6.1	± 1.8	0.01	-53.8	± 2.3	6	6.1	± 0.4	-1.9	± 0.6	0.03
		154	-7.0	± 2.1	0.01	-53.5	± 1.7	6	6.3	± 0.5	-1.6	± 1.3	0.42
		5 Rec	-0.6	± 0.8	0.24	-47.7	± 1.6	4	6.2	± 1.1	-1.8	± 0.9	0.26
	Steady state current	5				-49.3	± 0.8	7	6.8	± 0.4			
		40	-3.7	± 2.0	0.04	-54.2	± 1.9	5	6.2	± 0.5	-0.5	± 0.2	0.10
		154	-4.4	± 2.2	0.02	-55.0	± 2.4	5	7.9	± 0.7	1.2	± 0.9	0.25
		5 Rec	1.6	± 2.1	0.18	-47.7	± 0.1	5	7.3	± 0.6	0.5	± 0.5	0.28
KCNQ 2+3	Tail currents	5				-26.3	± 0.9	14	11.3	± 0.6			
		40	-6.4	± 0.6	0.01	-32.5	± 0.8	10	8.9	± 0.6	-2.4	± 0.4	0.01
		154	-10.3	± 0.7	0.01	-36.4	± 1.5	11	9.3	± 0.7	-1.9	± 0.5	0.01
		5 Rec	-1.7	± 1.0	0.23	-26.7	± 1.8	4	11.4	± 0.8	-1.1	± 0.6	0.11
	Steady state current	5				-32.9	± 0.9	10	7.2	± 0.4			
		40	-4.7	± 0.5	0.01	-37.6	± 1.1	9	6.8	± 0.6	-0.8	± 0.3	0.01
		154	-9.5	± 0.6	0.01	-42.4	± 1.8	10	8.4	± 0.4	-1.2	± 0.4	0.01
		5 Rec	-2.9	± 1.7	0.30	-36.2	± 4.1	3	31.2	±13.5	0.3	0.5	0.30

4.4.2 Change in E_K with current amplitude and duration

A constant problem in determining the voltage dependence of activation from tail currents was the non-tapering off of the tail current amplitude at positive test pulse potentials (see red trace in **fig. 17C**). This posed a problem when fitting sigmoid shaped Boltzmann functions to these curves.

Further, when calculating conductance from the steady-state currents (blue arrow in **fig. 17B**) and fitting voltage-conductance curves the value of E_K had to be manually read out in order to gain a sigmoid voltage-conductance relationship as described in section **4.3.3**. The value of E_K used in these calculations had to be estimated from the

reversal of current relaxation direction. This value always differed from the theoretical value calculated from the ion concentrations in bath and pipette.

A hypothesis that might explain these problems of non-tapering voltage-tail-current plots and E_K variations was a potassium accumulation at the extracellular membrane due to high experimental outward currents. Two experiments were conducted in order to test whether the ratio of extracellular to intracellular K^+ concentration changed during the experimental procedure. If the ion concentrations in the direct vicinity of the membrane changed due to a high experimental ion current, then this effect might be exacerbated by a further increase in current amplitude with more positive depolarisations or by increasing the duration of the ionic current. In one experiment depolarisation was increased to +160 mV and in the other E_K was estimated by a voltage ramp when increasing the time of depolarisation up to 10 s.

KCNQ2-mediated potassium outward current was increased by depolarising the membrane from -70 mV holding potential for one second in 10 mV increments up to +160 mV. The experiment was conducted in 5 mM $[K^+]_e$. When having plotted tail current amplitude against membrane voltage (red circles in **fig. 17C**) one could see that the inward tail current does not reach a maximum even after depolarisation to +160 mV. At the same time the steady-state outward current at the end of the 1 s depolarising pulse did reach a maximum as can be seen by tapering of current traces (blue arrow in **fig. 17B**).
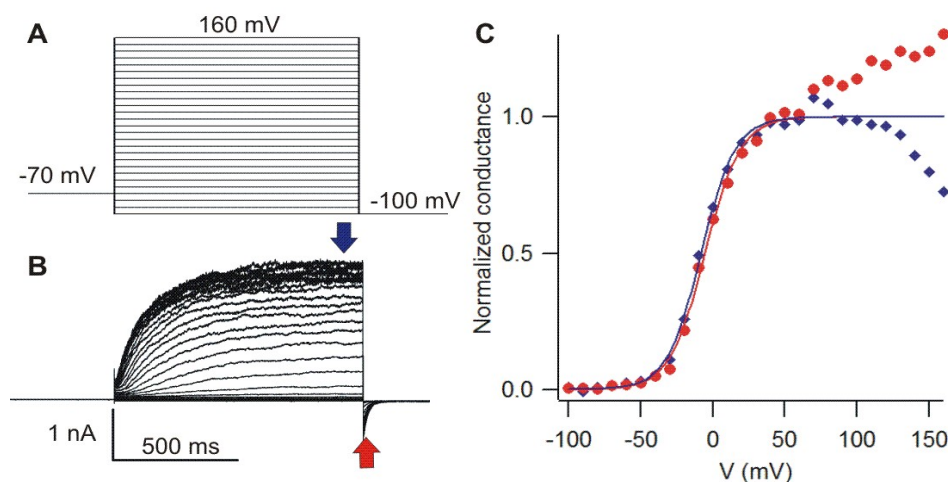
Fig. 17: Voltage-dependent conductance of KCNQ2 determined from tail currents and steady-state currents
The 3-step pulse protocol **(A)** applied to a KCNQ2 expressing CHO cell resulted in the recording of current traces shown in **(B)**. **(C)** Plot of conductance with increasing depolarisation from -100 mV to +160 mV calculated from steady-state current (blue) and tail current (red). The curve was fitted with a Boltzman function from -100 mV to +50 mV and normalized to the maximum of the fit.

These currents were then converted into conductance as described in section **4.3.3**. This conductance showed a decline at depolarising potentials positive to +90 mV (blue diamonds in **fig. 17C**).

In a second experiment E_K change was investigated by increasing the duration of outward current. E_K was determined from the change in direction of current in a voltage ramp following the depolarisation pulse in 5 mM $[K^+]_e$. After KCNQ2 activation by a depolarisation to +50 mV of variable duration between 10 ms and 10.3 s a voltage ramp changed the membrane potential from -40 mV to -90 mV within 100 ms. The pulse protocol and current trace can be seen in the inset of **fig. 18**. **Fig. 18** shows a plot of zero current potential determined by the voltage ramp against activation duration. Zero current potential determined by ramps becomes more positive with longer depolarisations to +50 mV when regarding nearly full activation at depolarisation times longer than 0.5 s.
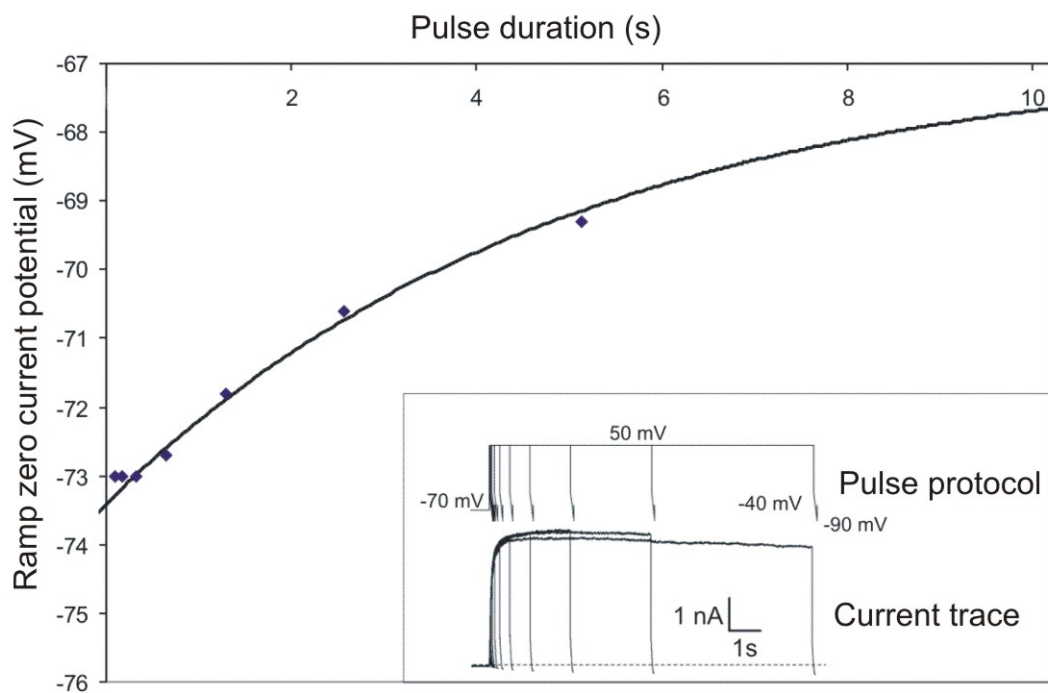
Fig. 18: Change in zero current potential with variable duration of KCNQ2 activation determined by voltage ramp protocols in 5 mM $[K^+]_e$
KCNQ2 expressing CHO cells were depolarised to +50 mV from a holding potential of -70 mV. The time of depolarisation was increased from 10 ms to 10 s. The membrane potential where the current changes direction from outward to inward was determined by a 100 ms voltage ramp from -40 mV to -90 mV following the depolarisation pulse. This zero current potential showed an increase when plotted against the test pulse duration that might be explained by an extracellular accumulation of K^+ ions.

These zero current potentials were exponentially fitted by V(t)=-73.4mV+6.6mV*(1-e^(-0.204s^{-1}*t)) (shown as a regression curve in **fig. 18**). This corresponds to an extrapolated zero current potential of -73.4 mV at t=0 s after no depolarisation and a zero current potential of -67.8 mV after a theoretical infinite duration of depolarisation.

Three assumptions were made. First, the intracellular K^+ concentration equals the K^+ concentration in the pipette (IC). Second, an absence of leak currents was assumed. Third, the zero current potential determined by voltage ramp protocols corresponds to the potassium equilibrium potential E_K. After correcting for the liquid junction potential, the extracellular potassium concentration was calculated from Nernst's equation from the experimentally determined E_K and $[K^+]_i$ of 156 mM at a room temperature of 23°C: E_K=-58.8mV * log $[K^+]_i$ /$[K^+]_o$. For t=0 $[K^+]_o$ was calculated to be 8,8 mM rising to 11,0 mM for t=∞. With this cell and its current amplitude $[K^+]_e$ shows a +2.2 mM increase in the cell surrounding with an increase in pulse duration of outward current by prolonged depolarisation pulses.

4.4.3 Rundown

Although some investigators have recorded KCNQ activation curves in conventional whole-cell patch (Punke and Friederich 2007; Wickenden et al. 2007), a rapid decrease in current amplitude was regularly observed (see **fig. 19**). This decrease in current amplitude impeded comparative measurements over time when exchanging bath solutions. A decrease in current amplitude or rundown can be due to the washout of intracellular substances by the much higher pipette volume. Rundown of KCNQ current is sensitive to intracellular signal cascades coupled to G_q proteins (Suh et al. 2004) and increased by PIP2 hydrolysis (Zhang et al. 2003). To prevent a concentration change of intracellular substances by conventional whole-cell washout (Marty and Neher 1983) a Nystatin-perforated patch was used (Horn and Marty 1988). This method uses chemicals inside the patch pipette which are incorporated into the cell membrane under the patch. It creates an electrical access to the inside of the cell by forming ion permeable pores without rupturing the membrane patch. The antibiotic Nystatin was applied in a concentration of 0.24 mg/ml as described in chapter **3.3.4**. The rundown in the perforated-patch mode was much slower than in the conventional whole-cell mode rupturing the patch membrane as can be seen in **fig. 19**.

A disadvantage of using the perforated patch is a relatively high series resistance R_s which creates higher potential errors compared to the conventional whole-cell patch technique. Therefore measurements were only started when R_s fell below 15 MΩ and in the majority of experiments R_s was between 5 MΩ and 10 MΩ when data were acquired. To gain an idea of the voltage error caused by the residual series resistance a simulation was carried out and will be described and discussed in sections **4.4.4** and **5.1.6**, respectively.
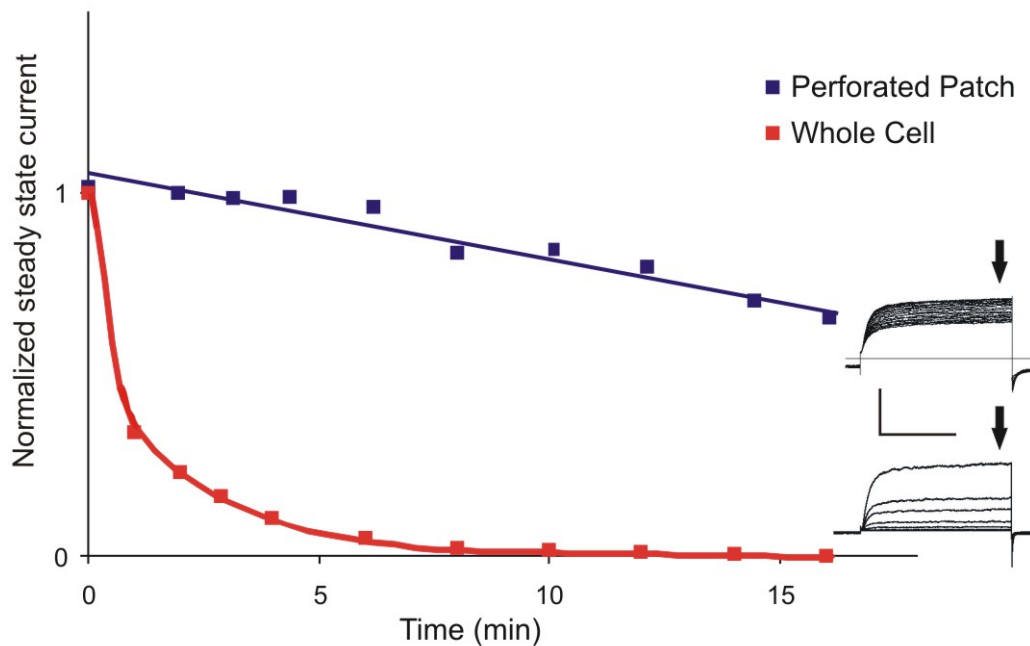
Fig. 19: Rundown in conventional whole-cell and Nystatin-perforated patch mode
KCNQ 2+3 transfected CHO cells were depolarised from -70mV to +50 mV for 1s. Current at the end of the depolarising pulse is plotted against time after start of measurement. The red trace shows a quick decrease (rundown) in current over time in conventional whole-cell mode rupturing the patch membrane. Rundown in Nystatin-perforated patch is much slower, blue trace. In conventional whole-cell time measurement was started after breaking through the patch membrane. In perforated-patch time measurement was started after reaching a series resistance below 30 MΩ. Pulses were started manually. Current traces are shown on the right. Arrow indicates point of current amplitude measurement. Scale bars represent 2 nA and 500 ms.

4.4.4 Simulation of the influence of series resistance error on activation curves

According to Ohm's law the voltage drops across a resistance in proportion to the size of resistance in ohms and current in amperes. Electrical access from the amplifier to the cell in patch-clamp experiment in not of zero resistance. That is why series resistance effects cause a difference between the real membrane potential V_m and the clamp potential V_{clamp} that is applied to the membrane via the amplifier. This

difference is proportional to the access resistance (R_s in **fig. 2**) and the amplitude of membrane current. Data analysis normally assumes that $V_m = V_{clamp}$ after using a hardware compensation process or series resistance compensation. But a small voltage error (**dV= V_{clamp} - V_m**) remains because compensation does not reach 100% which would cause oscillations and destruction of the highly sealed patch. In order to estimate the effect of residual series resistance after the hardware compensation, a simulation was conducted. Data points in KCNQ2+3 activation curves where corrected for these errors by calculations using excel spreadsheet. This was done for both the data obtained from steady-state current and tail current analysis.
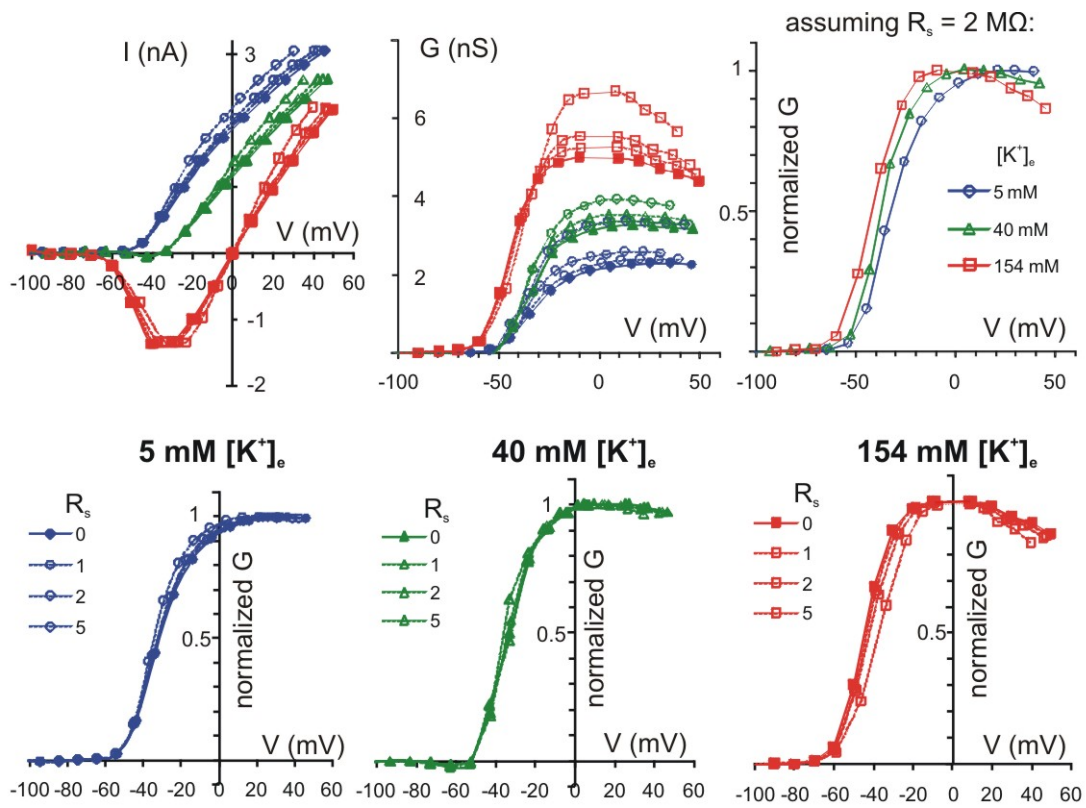
Fig. 20: Simulation of R_s corrected KCNQ 2+3 activation curves obtained from steady-state current analysis
3 scenarios assuming 1, 2 and 5 MΩ of series resistance R_s remaining after electronic series resistance compensation were used to calculate voltage clamp errors. In a computational simulation these residual R_s errors were compensated for and then plotted. Original data was plotted with full colour lines and symbols for different $[K^+]_e$ (blue = 5mM; green = 40 mM; red = 154 mM). Curves corrected for 1,2 and 5 MΩ remaining R_s error are shown with dotted lines between data points for current-voltage, conductance-voltage and normalized conductance plots. Assuming an access resistance of 10 MΩ and 80% R_s compensation, a realistic 2 MΩ residual R_s error would influence the results obtained for the voltage dependence of activation for KCNQ measurements. The figure on the upper right shows the curves as lines between data points after simulation and correction of this error for all 3 $[K^+]_e$. A negative shift in the voltage dependence of activation with rising $[K^+]_e$ can still be seen after correction for a residual series resistance error. $V_{1/2}$ and k values were determined by Botzmann fits (not shown) and are given in table 6.

Table 6: Calculated changes in KCNQ activation parameters assuming 1, 2 and 5 MΩ of series resistance remaining after electronic series resistance compensation with steady-state current analysis

$V_{1/2}$ and k were determined after correction for different magnitudes of remaining series resistance error R_s (MΩ) in 5, 40 and 154 mM $[K^+]_e$. Values for $V_{1/2}$ (mV) and slope factor k (mV) were determined by Boltzmann regressions from the data shown in fig. 20 and are given in the table.

R_s (MΩ)	$V_{1/2}$ (mV)			k (mV)		
	5	40	154	5	40	154
0	-29.4	-35.6	-44.4	7.7	6.8	6.5
1	-31.5	-32.6	-43.9	8.8	7.3	6.1
2	-32.0	-38.2	-41.7	8.5	6.7	7.1
5	-33.5	-33.7	-36.6	7.5	6.2	8.0

In the already described experiments electronic compensation for series resistance by pulse software and patch-clamp amplifier was between 70% and 90%. Assuming an average series resistance compensation of 80%, the other 20% cause a voltage error dV. Assuming an average access resistance of 10 MΩ in perforated-patch mode, one can calculate the voltage error dV from the current measured. For example 3 nA KCNQ outward current at +50 mV in 5 mM $[K^+]_e$, with a series resistance R_s of 10 MΩ 80% compensated would cause a voltage error dV of 6 mV (dV=3 nA * (10 MΩ * 20%)). The actual membrane potential for 3 nA of current measured is only +44 mV (V_m) instead of +50 mV (V_{clamp}) as shown on the screen to the experimenter by the patch-clamp software.

Voltage error corrections were performed exemplary for mean values of KCNQ2+3 experiment data. Three scenarios assuming different values of series resistance were chosen to observe the effect of series resistance on the interpretation of KCNQ2+3 current data. 1, 2 and 5 MΩ of residual R_s after hardware compensation were assumed and I/V- and G/V- plots were corrected for the voltage error dV. **Fig. 20** shows original KCNQ2+3 data obtained from steady-state current analysis colour coded for 5, 40, 156 mM $[K^+]_e$. The dotted lines in the first two figures represent current-voltage and conductance-voltage data after simulated correction for 1, 2 and 5 MΩ of series resistance. Computational correction for series resistance results in steeper current voltage relationships which would correspond to a smaller value of k. Activation curves were also shifted horizontally depending on E_K and the direction of current dependent on $[K^+]_e$ as can be seen in **Fig. 20**. Boltzmann fits confirmed this observation: Assuming a maximal residual R_S of 5 MΩ after hardware compensation $V_{1/2}$ shifted with respect to the original data: left by -4 mV in 5 mM $[K^+]_e$ and right

by +7.8 mV in 154 mM $[K^+]_e$. A change in steepness of curve after computational R_s correction was small. Exact values calculated from the simulation can be found in **table 6**.
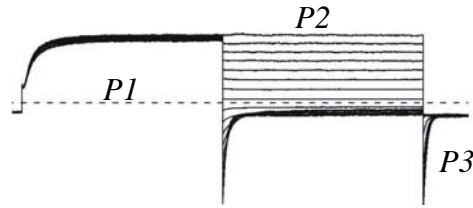
In contrast to computational correction of activation curves obtained from steady-state currents the simulation was more complicated for tail currents. Here two series resistance errors add together – during P2 and P3. After activation of KCNQ current by the depolarising test pulse P1 a series resistance error occurs during test pulses P1 and P2 as well as in rapid hyperpolarisation to -100 mV tail potential P3, depending on the size of current amplitudes. The voltage error during test pulse P2 has been calculated as described above for steady-state currents. An additional tail current potential error during P3 caused the tail potential to be less than the ideal -100 mV expected by the experimenter. This potential error changed with tail current amplitude depending on two factors: the degree of channel activation and the potassium equilibrium potential. First, tail current was larger with increasing channel activation depending on test pulse potential P2. Second, tail current was the larger the further the pulse potential P3 differed from E_K in different $[K^+]_e$.

In order to conduct the simulation and to correct for series resistance errors in tail current analysis an ideal tail current was calculated. This ideal tail current could have been seen if there had been no series resistance error with inward tail currents. This ideal tail current was extrapolated from the measured tail current amplitude by calculation and computational correction for series resistance:

The calculated ideal tail current amplitude **I_{Tcal}** mirroring tail current at an ideally constant potential **V_{Tideal}** of -100 mV during P3 was calculated: Due to the series resistance error the real potential during P3 **V_{Treal}** was less negative than V_{Tideal} (-100 mV) by a potential error **dV_T** depending on measured tail current amplitude I_{Trec}. Recorded tail current **I_{Trec}** was smaller than the ideal tail current I_{Tcal} at -100 mV by a factor **$F_{correction}$** that had to be corrected for.

$$I_{Tcal} = I_{Trec} * F_{correction}$$

This correction factor is the ratio of ion driving potential for an ideal tail current at -100 mV (dE_{T-100}) to the really clamped ion driving potential (dE_{Tclamp}). dE_{Tclamp} deviates from -100 mV by the voltage error dV_T (defined above) due to the series resistance error.

$$F_{correction} = \frac{dE_{T-100}}{dE_{Tclamp}}$$

The ideal ion driving potential dE_{T-100} is the difference between the ideal potential at P3 (-100 mV) and E_K depending on the extracellular potassium concentration. E_K was -76 mV for 5 mM $[K^+]_e$, -27.3 mV for 40 mM $[K^+]_e$ and -0.3 mV for 154 mM $[K^+]_e$ as used in the calculation of whole-cell conductance (section 4.3.3) .

$$dE_{T-100} = -100mV - E_K$$

The real ion driving potential at P3 dE_{Tclamp} is smaller than the ideal dE_{T-100} due to the series resistance error. It can be calculated as the difference between the real voltage clamp potential V_{Treal} and E_K.

$$dE_{Tclamp} = V_{Treal} - E_K$$

The real potential driving the tail current at P3 V_{Treal} can be calculated subtracting the potential error dV_T from the ideal potential of -100 mV.

$$V_{Treal} = -100\ mV - dV_T$$

The potential error during P3 dV_T can be calculated by Ohm's Law from the recorded tail current amplitude I_{Trec} assuming different series resistances R_s.

$$dV_T = I_{Trec} * R_s$$

A residual series resistance after electronic compensation of 1, 2 and 5 MΩ was simulated as done for the steady state current analysis described in the first part of this chapter. Summing up all calculatory steps gives a formula for calculating the size of the ideal tail current from the measured tail current amplitude having compensated for the residual series resistance errors:

$$I_{Tcal} = I_{Trec} * \frac{-100\ mV - E_K}{-100\ mV - E_K - \left(I_{Trec} * R_s \right)}$$

Calculations assuming different residual series resistance errors (1, 2, 5 MΩ) were done for each amplitude of tail current and at different $[K^+]_e$. The pretail potential P2 was corrected for as described in the simulation of steady-state currents. **Fig. 21** shows the result of simulating a residual series resistance and correcting for it in KCNQ activation curves from tail current analysis.

The changes in $V_{1/2}$ and k (**table 7**) after correction for residual series resistance error did not differ to a high degree from those described for the same simulation done for KCNQ activation curves determined from steady-state conductance (**table 6**).

The effects of a remaining series resistance error after electronic compensation by HEKA hard- and software in KCNQ experiments with high amplitude currents were evaluated by conducting a computational simulation. In 3 scenarios assuming different magnitudes of residual series resistance error the experimental data was corrected for these errors in order to see their relevance for the interpretation of the experimental results. The simulation showed that part of the negative shift in voltage dependence of KCNQ activation found by this experimental investigation can be explained by series resistance error effects due to the high amplitude of non-inactivation KCNQ currents.
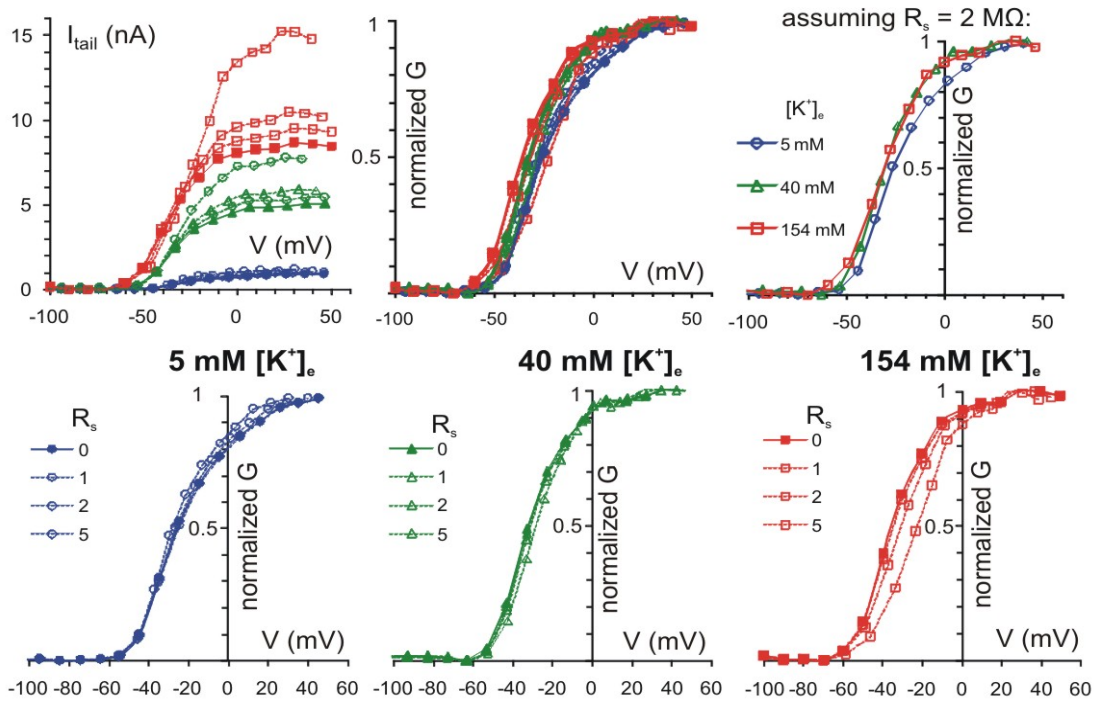
Fig. 21: Simulation of R_s corrected KCNQ 2+3 activation curves obtained from tail current analysis

When determining the voltage dependence of activation of KCNQ by analysing tail currents two errors add due to remaining uncompensated R_s. The voltage during the test pulse interval P2 changes due to the uncompensated R_s as already explained in the first section of the chapter. When analysing tail currents a second error due to uncompensated R_s during the test pulse P3 has to be taken into account as well. Three scenarios assuming 1, 2 and 5 MΩ of remaining series resistance R_s after electronic series resistance compensation were used to calculate voltage clamp errors and to extrapolate tail current for an ideal test pulse potential P3 of -100 mV. Values corrected for this error were then plotted and are shown as dotted lines between points. Original data was plotted with full colour lines and symbols for different $[K^+]_e$ (blue = 5mM; green = 40 mM; red = 154 mM). The figure on the upper right shows voltage conductance relationships compensated for a realistic remaining series resistance error of 2 MΩ.

Table 7: Calculated changes in KCNQ activation parameters assuming 1, 2 and 5 MΩ of series resistance remaining after electronic series resistance compensation for tail current analysis

Voltage of half maximal activation $V_{1/2}$ (mV) and slope factor k (mV) were determined from Boltzmann fits (not shown) for the data shown in fig. 21 and after correction for different magnitudes of residual series resistance errors R_s (MΩ) remaining after electronic series resistance compensation in 5, 40 and 154 mM $[K^+]_e$.

R_s (MΩ)	$V_{1/2}$ (mV)			k (mV)		
	5	40	154	5	40	154
0	-26.3	-32.5	-36.4	12.0	9.4	10.1
1	-25.8	-31.8	-36.4	12.2	9.6	10.1
2	-27.2	-31.0	-31.6	11.3	9.7	10.4
5	-28.8	-28.7	-23.9	10.4	9.4	10.5

5 DISCUSSION

This work discusses the investigation of heterologously expressed KCNQ channels and their current in increasing extracellular potassium concentration.

Several methodical difficulties were encountered that required correction procedures. These procedures were developed in the context of this experimental investigation and are substantial in evaluation of the acquired data. Therefore a discussion of methodical challenges will be presented first.

Second, a discussion of extracellular potassium concentration effects on KCNQ current characteristics will follow with regard to the voltage dependence of activation, the kinetics of KCNQ activation and deactivation, and whole-cell conductance.

In a third part physiological and pathophysiological consequences of these effects will be discussed.

5.1 Methodological aspects in measuring KCNQ activation in changing $[K^+]_e$

Several problems emerged when trying to reproduce the voltage shift in increasing $[K^+]_e$ of KCNQ activation found in K^+ currents at the node of Ranvier (Schwarz et al. 2006). Only perforated-patch recordings with an adapted voltage protocol provided reproducible currents that could be examined by different approaches of data analysis. A change in K^+ concentration caused an alteration of the reversal potentials and influenced the corrections for series resistance and liquid junction potentials.

The method commonly used for determining voltage dependence of KCNQ current activation is the analysis of tail currents at -100 mV directly following a 1 s variable activating voltage pulse from a holding potential of -70 mV. This way of characterising KCNQ activation was used to first describe the molecular correlate of the M-current (Wang et al. 1998) and has been used in a similar fashion ever since (Selyanko et al. 2000; Suh and Hille 2007).

5.1.1 Rundown

When trying to investigate KCNQ currents with this protocol in conventional whole-cell mode a strong decline in the amplitude of current was observed. KCNQ current

disappeared within several minutes as could be seen in fig. 19. Using Nystatin-perforated patch (Horn and Marty 1988) permitted to measure relatively stable KCNQ currents. In order to control for the stability of the current during the experiment an additional constant 1 s depolarising pulse to +50 mV was used preceding every variable voltage pulse (Tatulian et al. 2001). Only those experiments were analysed which showed a constant current for the whole duration of the voltage protocol. An explanation of this rundown phenomenon is modulation of KCNQ current by intracellular messengers. Rundown of KCNQ current due to phosphatidylinositol 4,5-bisphosphate PIP_2 hydrolysis has already been described (Zhang et al. 2003).

The pipette volume is much bigger than the cell volume and dilutes the concentration of intracellular messengers associated to KCNQ. This results in an exponential like time course of current decline when using conventional whole-cell patch. But even in Nystatin-perforated patch, current rundown was observed. This rundown of current was much slower and had a rather linear time course as shown in fig. 19. Nystatin pores incorporated into the membrane allow electrical access from the pipette to the cell by being permeable to different ions. Thereby this method might disturb sensitive intracellular balances influencing KCNQ such as Ca^{2+} (Selyanko and Brown 1996), Calmodulin (Gamper and Shapiro 2003), Mg^{2+} (Suh and Hille 2007) and G-proteins (Pfaffinger 1988). These disturbances can be the cause of the linear rundown of current observed.

5.1.2 Non-saturation of activation curves obtained from tail current analysis

Tail current analysis is a practical approach in order to describe voltage-dependent KCNQ activation. In the used pulse protocol tail current at -100 mV represents the level of conductance during the preceding variable voltage pulse and is comfortable to measure as KCNQ shows a rather slow time course of deactivation. In the case of KCNQ2 and KCNQ3, no inactivation occurs, whereas KCNQ5 shows some recovery from inactivation at tail amplitudes of -100 mV before deactivation occurs and has been described in prior publications (Jensen et al. 2007). The process of subtracting leak current and the estimation of the exact E_K can be neglected using this method as it remains constant at a constant potential of -100 mV during the pulse interval P3. This makes tail current analysis preferable to direct examination of conductance at

the end of the variable voltage pulse. When fitting tail current amplitude against the potential during P2 a sigmoid arrangement of data points represents voltage-dependent activation of KCNQ macroscopic conductance with a saturation of activation at positive membrane potentials (Selyanko et al. 2000).

Fitting the acquired data points derived from the experiments described, tail current amplitude of KCNQ2 and KCNQ3 subunit currents did not show complete saturation even at very positive voltages. This problem of non-saturation seemed to be encountered before when looking at activation curves in earlier publications using this method (Wang et al. 1998; Wickenden et al. 2007). A practical approach seemed to be defining tail current amplitude with a preceding depolarisation to +50 mV as 100%, normalizing to it and fitting a Boltzmann function to this maximum (Selyanko et al. 2000; Suh and Hille 2007; Tatulian et al. 2001).

This non-saturation of tail currents during depolarisation could be explained by either intrinsic properties of KCNQ channels or might be due to external factors such as the experimental procedure of investigating voltage-dependence of activation with heterologously expressed ion channels.

Two intrinsic channel properties that might have explained the observed phenomenon of non-saturating tail currents were an additional increase in open-probability or additional conductance states of the channel. On the one hand single channel recordings of KCNQ2 and KCNQ3 have shown an open probability of only 6-10% at 0 mV (Selyanko et al. 2001) hypothetically leaving the potential of much higher channel open-probabilities that might then result in an further increase in the channels' ion-conductance at positive membrane potentials. One the other hand additional conductance states of KCNQ channels have been described for KCNQ1 (Yang and Sigworth 1998) and KCNQ2+3 (Selyanko et al. 2001). These additional conductance states showed a rather small conductance and were negligible as they occupied less than 1% of open states at a membrane potential of 0 mV. These two intrinsic hypotheses explaining the non-saturation of tail currents remain speculative and would need a variety of additional techniques and experimentation for clarification.

External causes that result in the observed non-saturation of tail currents at positive membrane potentials might lie in the experimental procedure of investigating heterologously expressed ion channels. A change in E_K due to a change in ion

concentrations around the membrane with high experimental currents could explain the non-saturation of tail current during depolarisation as KCNQ current show no or only little inactivation resulting in high ion currents. In order to test this hypothesis and to crosscheck the results a second method of deriving activation curves from the recordings was used. Activation curves were determined from the whole-cell conductance of steady-state currents. The results of this second method were then compared to the already described results from the analysis of tail currents. If both modes of analysis showed non-saturation of activation curves, intrinsic channel properties as an explanation for the non-saturation would become more likely. If not, non-saturation of tail currents would be a result of the procedure of experimentation. The conversion of steady-state current to conductance was not as uncomplicated as expected. A discussion of this procedure will therefore come next before a discussion of the changes in E_K due to the experimental procedure and a comparison of the two methods of analysing tail currents vs. steady-state currents and its implications can follow.

5.1.3 Correction in steady-state current analysis

Before obtaining a sigmoid conductance-voltage relationship from steady-state current at the end of the variable voltage pulse in the pulse protocol, two correction procedures were necessary as described in chapter 4.3.3 taking into account leak currents and changes in E_K.

Steady-state currents recorded at the pulse interval P2 (see fig. 3) had to be corrected for non KCNQ specific leak current. During tail current analysis, this leak was constant with a constant potential during P3 at -100 mV for all sweeps. Therefore the constant leak could be neglected in tail current analysis. On the contrary for steady-state current analysis this leak changed with each membrane potential and had to be accounted for when handling KCNQ specific current. Examination of non-transfected CHO controls showed the non-specific leak current to be linear with different membrane potentials and increasing in high extracellular potassium concentrations (chapter 4.2).

Causes for these leak currents are endogenous ion channels in the membrane of CHO cells. Another component of non-specific current is leak in the classical sense by ions moving around the seal between pipette and membrane. CHO cells have been described to show Ca^{2+} activated cationic conductance (Gamper et al. 2005), TRP (Vaca and Sampieri 2002) and cell swelling-activated chloride channels (Li et al.

2000). Cell swelling (Nichols et al. 1995) might occur when increasing $[K^+]_e$, but an increase in volume of the CHO cells, and indicator of osmotic changes, was not observed through the microscope after solutions had been exchanged. Changes in endogenous CHO currents have to be taken into account, if present, when testing a rise in $[K^+]_e$ on over-expressed KCNQ channels.

Control measurements in non-transfected CHO cells (fig. 4) showed that the sum of leak current reversibly rises with $[K^+]_e$. Controls also showed a linear change of non-specific currents with membrane potential and no observable kinetic behaviour of activation or deactivation. Therefore a linear correction of non-specific KCNQ current was conducted as described in chapter 4.3.3.

5.1.4 Changes in E_K

After the procedure of correcting for leak-currents a second procedure correcting for changes in E_K was necessary before obtaining activation curves from whole cell conductance calculations.

KCNQ currents corrected for non-specific leak and converted into conductance still did not show a sigmoid conductance-voltage relationship. The curves rather showed large deviations around E_K for each different $[K^+]_e$. E_K had been calculated by Nernst's equation from ion concentrations, that were present in experimental bath and pipette solutions. Only after assuming that E_K was up to 10 mV more positive than expected from calculations, data points yielded a sigmoid curve. These more positive E_K values for conversion of current to conductance data were estimated from the reversal of potassium current relaxation direction (fig. 11E). The discrepancy of E_K between estimates from the current traces and calculation was smaller for higher $[K^+]_e$ and was 0 for 154 mM $[K^+]_e$. One has to bear in mind that the reversal of current might not be exactly E_K as small Na^+ conductance of the membrane causes a deviation of E_{rev} to more positive values than E_K (Nichols et al. 1995). Another influencing factor is that the selectivity of K^+ channels (Hille and Schwarz 1978) and KCNQ2+3 channels in particular (Prole and Marrion 2004) is not absolute for potassium.

Assuming that ion concentrations in solutions were correctly prepared, a deviation of E_K from the value expected can be caused by changes in the ion concentrations around the membrane during the experimental procedure. On the one hand a depletion of intracellular K^+ during high experimental outward current might have caused this positive shift. Although intracellular K^+ ions are not significantly

depleted during physiological outward currents, this might be the case under experimental conditions. On the one hand the pipette serves as a big reservoir for intracellular ions under experimental conditions. On the other hand a rise in the extracellular potassium concentration in the direct vicinity of the membrane might have caused E_K to be more positive than expected from the ion concentrations in the solutions prepared.

To test the first hypothesis of intracellular K^+ depletion a thought experiment was conducted. A priori, during an unphysiologically high 1 s outward membrane current of 3 nA as observed for KCNQ2 the cell interior would lose 3 nC of charge (I=q/t; I current, q charge, t time). Assuming a diameter of approximately 10 μm and spherical shape of the cell this would correspond to a cell volume of 524 $μm^3$ or 524 fl (V=4/3$πr^3$; V volume, r radius). With a $[K^+]_i$ of 156 mM as in the pipette the cell interior contained 7.33 mC of K^+ charge. Therefore the charge of K^+ ions in the cell would be 10^6 times greater than the charge lost through outward current – and this still disregards the patch pipette connected to the cell interior with an ion reservoir several times greater than that of the cell. A depletion of intracellular K^+ by outward current therefore seems unlikely to be a reason for a difference in E_K between calculated and empirically found values.

A second idea was that K^+ ions might have accumulated at the outer membrane giving rise to higher $[K^+]_e$ in the direct vicinity of the outer membrane than actually present in bath solutions and thereby shifting E_K to more positive potentials. Two components might have played a role in this: First, according to the disputed "electrolyte exclusion model" higher positive ion concentrations arise at the outer membrane due to negative surface charges of the cell membrane (Gilanyi et al. 1988). Second, although ion diffusion is quick, 1.96 $μm^2$/ms for K^+ (Hille 2001), unphysiologically high KCNQ outward current during experiments might have caused K^+ ions to accumulate in the direct vicinity of the outer channel pore. This would have led to higher $[K^+]_e$ encountered by the cell membrane than the concentration actually present in the surrounding bath. This effect should have increased with each further depolarisation generating more and more outward current.

Two experiments were conducted to test for a shift in E_K by high outward ion flux: In the first experiment, a longer depolarisation and outward ion flux will shift E_K to more positive potentials if K^+ accumulates at the outer membrane (chapter 4.4.2).

Voltage ramps following an increasing duration of full activation (fig. 18) showed an increasing but saturating shift in E_{rev} of about 6 mV with increasing pulse duration.

In a second experiment non-saturation of inward tail current was mirrored by a "over saturating", declining outward conductance during the pulse interval P2. With increasing outward current, E_K becomes more positive as $[K^+]_e$ increases due to accumulation on the outer membrane. Because of that shift in E_K, the ion driving force for outward current and with it outward steady-state conductance should decrease whereas inward tail current should increase at the same time. This was confirmed by the experiments when comparing whole cell conductance during P2 vs. tail currents during P3 (fig. 17).

In summary extracellular potassium accumulation with high outward ion flux caused a positive shift of E_K of up to 6 mV in 5 mM $[K^+]_e$. The rest of the deviation of E_{rev} from E_K could be explained by small Na^+ conductance as have been described in prior publications (Nichols et al. 1995). For higher $[K^+]_e$, the relative effect of extracellular K^+ accumulation was smaller in relation to the absolute $[K^+]_e$. These effects must be taken into account when exact characterization of ion channels showing high experimental currents such as non- inactivating KCNQ is of interest.

This comparison of steady-state conductance to tail conductance gave an explanation to the problem of non-saturating tail currents. Non-tapering of tail currents is rather a result of the experimental method of channel overexpression generating non-physiological high ion currents than being an intrinsic property of the ion channel itself. This might be an important point to take into consideration as tail current analysis is a standard procedure in characterisation of KCNQ, M-current and other ion channel analysis.

5.1.5 Characterisation of KCNQ activation curves as determined from tail current vs. steady-state current

Voltage dependence of KCNQ channel activation was obtained by two different approaches of current analysis. After correction for leak currents and changes in E_K, sigmoid conductance-voltage relationships were obtained from steady-state currents at the end of the variable voltage pulse (P2). By fitting these with a Boltzmann function, characteristics of activation such as $V_{1/2}$ and the slope factor k of activation were compared to results from tail current analysis (fig. 14).

$V_{1/2}$ obtained from steady-state currents were at significantly more negative potentials than those obtained from tail currents. Regarding the steepness of activation curves, slope factor k was significantly smaller or, in other words, the activation curves were steeper obtained from steady-state current than those obtained from tail current analysis (fig. 15). A reason for the different values of $V_{1/2}$ obtained from the two modes of analysis is the way of fitting conductance curves. As tail current amplitude does not saturate at most positive potentials, fitting a Boltzmann function tends to fit the curve more to the right (fig. 14) where the maximum lies at a cutoff voltage (in this case: +50 mV; $I_{max}=I_{(50mV)}$). This approach has been taken in most prior publications investigating KCNQ activation (Schwarz et al. 2006; Suh and Hille 2007; Tatulian et al. 2001). In contrast to tail current analysis, fitting conductance curves from steady-state currents tends to fit the activation curves more to the left as a maximum amplitude was reached at potentials negative to +50 mV. Activation curves from steady-state current analysis are steeper than tail current activation curves, for the same reason. As the minimum of the sigmoid curves stays the same in both modes of analysis, the different maxima described above result in a different steepness or k of the Boltzmann fit. The difference in $V_{1/2}$ and k obtained from both modes of analysis could thereby be explained by the already discussed problem of K^+ accumulation due to high, experimental, non inactivating KCNQ currents resulting in different shapes of the activation curves and therewith its Boltzmann regression plots.

The differences in $V_{1/2}$ comparing both modes of analysis were more pronounced for KCNQ2 and KCNQ2+3 than for KCNQ3 (fig. 15). As KCNQ3 expression yielded a smaller overall current amplitude compared to other KCNQ subunits, this observation is consistent with the effects of extracellular K^+ accumulation discussed above. A factor influencing these differences between the results of high- and low-magnitude KCNQ subunit current amplitudes is the series resistance error. This error is proportional to the magnitude of current measured in voltage-clamp experiments. The tail current amplitude in isotonic $[K^+]_e$ was larger compared to the preceding current during P2, increasing the series resistance error. With a higher amplitude of tail current causing a higher series resistance error the membrane voltage in high $[K^+]_e$ seemed to be more negative as it actually was. This error makes the voltage shift in activation to appear greater in tail current analysis than with steady-state

current activation analysis. Series resistance errors will be discussed further in the following chapter.

Both modes of analysing KCNQ activation have their advantages and pitfalls. To determine the voltage dependence of activation by analysing tail currents is more straightforward with respect to data handling. Conversion of currents into conductance is not necessary here. Tail current analysis at -100 mV becomes more inaccurate though in high $[K^+]_e$ as tail currents at -100mV increase in amplitude and generate increasing voltage errors due to uncompensated series resistance.
On the other hand, the analysis of voltage dependence of activation from steady-state currents is more difficult in data handling. Before gaining sigmoid relationships of voltage dependence of activation, manual procedures of leak and E_K corrections make this method uncomfortable in data handling and are an additional source of systematic errors. Information about absolute outward whole-cell conductance is gained though. This is an additional physical characteristic that cannot be explored in such a way from tail current analysis.

Altogether comparing both modes of analysis enhances the understanding of deviations from model behaviour when analysing activation of KCNQ currents and sharpens the viewpoint for limitations to the experimental procedure. Voltage dependence of activation showed differences in position and shape of the activation curves using different methods of analysis. At the end a change in the voltage dependence of activation in increasing $[K^+]_e$ could be confirmed by comparison of both methods of analysis.

5.1.6 Series resistance

According to Ohm's law, a voltage drop occurs across a resistance proportional to the magnitude of current. In perforated-patch clamp the access resistance is not negligible causing the membrane potential to differ from the clamp potential applied to the membrane by the amplifier (Marty and Neher 1983). The electronic series resistance compensation of the HEKA amplifier and software diminished this error. In the experiments, electronic series resistance compensation was 70-90%, leaving about 20% of the error uncompensated. Normally this remaining resistance is ignored. But having a KCNQ current of high amplitudes of 3 nA after full activation, these 20% is not completely negligible.

In order to evaluate the influence of this uncompensated series resistance R_S on the results, a simulation of R_S error effects was performed using Excel spreadsheet calculations (chapter 4.4.4). A realistic remaining R_S of 2 MΩ was assumed after 80% electronic compensation and an average access resistance of 10 MΩ during the measurements. Simulation of the results was also conducted for 1 and 5 MΩ of residual R_S. The simulation performed was exemplary for data obtained for KCNQ2+3 activation analysis both from steady-state (fig. 20) and tail currents (fig. 21).

Activation curves were found to be shifted due to R_S error to more positive potentials with outward currents in low $[K^+]_e$ and to more negative potentials with inward currents and high $[K^+]_e$. The magnitude of this shift due to R_S error increased with the magnitude of current in concordance with Ohm's law.

For the analysis of tail currents two R_S errors add. First, the membrane potential during the variable voltage pulse is affected by the same voltage error as just discussed for steady-state current analysis. Second, there is an additional voltage error during pulse interval P3 increasing with the size of the tail current, which depends on both the level of KCNQ activation and on the magnitude of the driving ion force changing with $[K^+]_e$.

A simulation of residual R_S error effects was carried out for results gained from KCNQ2+3 co-transfected CHO cells generating the highest absolute currents. A shift in activation due to $[K^+]_e$ was also found for KCNQ3 currents which were smaller in magnitude than KCNQ2+3 currents. Here residual R_S error effects had less influence on the results than with high currents. Assuming a realistic remaining R_S of around 2 MΩ, a minor part of the negative shift in voltage of activation found in increasing $[K^+]_e$ could be explained by a residual series resistance error.

5.1.7 Liquid junction potential

Liquid junction potentials occur due to different mobilities of ions at interfaces between solutions containing different ion concentrations. In patch-clamp recordings such liquid junctions occur between pipette and bath as well as between bath electrode, agar bridge and bath. It is standard procedure that potentials measured or applied in voltage clamping are relative to zero current potential, calibrated at the beginning of the experiment when the pipette is in the bath. As bath ion concentrations are not equal to intrapipette ion concentrations a liquid junction potential adds to an offset potential that is calibrated as zero current potential (Neher

1992). This liquid junction potential is eliminated from the measurements from the point in time of attachment of the pipette to the cell membrane. A liquid junction potential error is therefore present during the following voltage clamp experiments if it is not corrected for. This error is often neglected as it stays almost constant whilst changing the experimental parameter to be investigated.

In the experiments described here the changing parameter is extracellular potassium concentration which causes liquid junction potential error to change during $[K^+]_e$ change. Therefore, liquid junction potentials were measured as described (Ng and Barry 1995) and subtracted offline when analysing recorded data. Maximal liquid junction error was measured to be about 4 mV between both 5 mM and 154 mM extracellular solutions against the reference. No correction of this liquid junction would cause misinterpretation of the shift in half maximal activation to be 4 mV greater than it really is between 5 and 154 mM $[K^+]_e$.

Liquid junction potential errors were corrected offline in the analysis of voltage dependence of activation. This correction was not conducted when comparing the voltage-dependent time course of activation, deactivation and whole-cell conductance changes due to practicality and necessity. In the analysis of whole-cell conductance (section 4.3.3) in different $[K^+]_e$, the interest of investigation rested rather in the magnitude of conductance changes than in the exact voltage dependence. Where the voltage dependence was of interest liquid junction potentials were taken into account by offline correction. In the kinetic analysis of KCNQ activation and deactivation, offline liquid junction potential correction did not allow direct comparison of time constants in different $[K^+]_e$ at each voltage. Therefore liquid junction potential effects were neglected comparing the values of the time constants of KCNQ activation and deactivation in different $[K^+]_e$. This poses a limitation on the statistical significance of effects found for the kinetics of KCNQ behaviour.

Liquid junction potentials have to be kept in mind especially when the bath solution with its ion concentrations is changed during an experiment. During this research, liquid junction potentials were taken into consideration where parameters such as activation, conduction and kinetics of KCNQ behaviour were evaluated in changing ion concentrations.

5.1.8 Donnan potential

Donnan potentials arise from the uneven distribution of ions due to the selective permeability of a membrane. When using a Nystatin-perforated patch this kind of potential develops between pipette interior and the intracellular space separated by the perforated membrane patch. The cell membrane under the patch pipette containing Nystatin pores is selective to monovalent cations such as Na^+ and K^+ as well as to Cl^- to a lesser extent. Intracellular proteins carrying negative charges do not cross Nystatin pores. In a model (Horn and Marty 1988), the cell interior was calculated to be -8.8 mV more negative than the voltage clamp patch pipette due to the Donnan effect. This effect contributes to the explanation of experimental potassium reversal potential being approximately 12 mV more positive than that calculated from ion concentrations alongside the effects of series resistance errors and extracellular K^+ accumulation discussed previously.

Donnan potenials might have affected the shift in activation found by increasing $[K^+]_e$ if the Donnan potential changed with a rise in $[K^+]_e$. Higher $[K^+]_e$ changes the equilibrium of ions across the membrane. K^+ and Cl^- influx could have caused water to follow by osmosis changing intracellular protein and chloride concentrations. One step further these might have changed the Donnan potential across the Nystatin patch as Nystatin is impermeable to proteins and also partly to chloride. As no cell swelling was observed during the experiments increasing $[K^+]_e$, this Donnan potential error was neglected when evaluating the parameters investigated. To exactly determine the effects of Donnan potentials is difficult and remains speculative in the context of this investigation.

Donnan potentials arise in perforated-patch clamp mode. They give a further explanation in deviations found in reversal potentials but were neglected in the analysis of changes in KCNQ behaviour with extracellular K^+ changes.

In summary, the major objective of this investigative work was to characterise activation of heterologously expressed KCNQ channels in increasing $[K^+]_e$. To accomplish this task, several methical obstacles had to be overcome. Only Nystatin-perforated-patch and an adapted pulse protocol allowed the measurement of stable KCNQ currents. Standard analysis of tail currents as well as the analysis of steady-state currents were the approach to evaluate and check the characteristics of KCNQ activation properties found in rising $[K^+]_e$. Data obtained from these methods

of analysis had to undergo correction. Procedures for leak current, potassium equilibrium and liquid junction potential changes were developed, applied and series resistance errors were simulated by scenario analysis. Only by taking into account these aspects of technical difficulties the results of KCNQ activation analysis in increasing $[K^+]_e$ can be thoroughly interpreted and evaluated. After the correction of these potential sources of error a residual but small shift in voltage dependence of activation in rising $[K^+]_e$ can be assigned to the biophysical properties of the ion channel or the membrane.

5.2 Influence of $[K^+]_e$ on KCNQ channel activation and deactivation

The objective of this investigation was to analyse the influence of $[K^+]_e$ on the biophysical properties of KCNQ channels. The increase in $[K^+]_e$ induced a significant shift in voltage dependence of activation to more negative potentials in all KCNQ channels investigated. In addition, an acceleration of activation and deactivation at membrane potentials positive to -40 mV and a slowing of deactivation at membrane potentials negative to -80 mV was found in KCNQ2+3. KCNQ2, KCNQ3 and KCNQ2+3 exhibited an increase in whole-cell conductance in high $[K^+]_e$.

5.2.1 Shift in voltage dependence of activation

CHO cells, transfected with one type of subunit of KCNQ2, KCNQ3 and KCNQ5 as well as co-transfected with KCNQ2+3 and KCNQ3+5, were investigated by perforated-patch clamp experiments. Two methodical approaches were used to determine voltage dependence of activation in KCNQ channel current. Both tail currents as well as steady-state conductance yielded activation curves which could be fitted by Boltzmann functions.

All subunit KCNQ currents did show a different voltage dependence of activation (table 5, fig. 6, fig. 7, fig. 14) as has already been described (Schroeder et al. 2000; Selyanko et al. 2000).
KCNQ2 $V_{1/2}$ values were between those described in the literature with $V_{1/2}$ determined from tail currents being more positive than $V_{1/2}$ determined from steady-

state currents whereas k values were almost identical (Biervert et al. 1998; Selyanko et al. 2000; Tatulian et al. 2001). $V_{1/2}$ values from the two modes of analysis showed a difference of 7 mV.

KCNQ3 $V_{1/2}$ values in contrast were equal with both modes of analysis and more negative than described in the literature. The slope in voltage dependence of activation was comparable to k values published (Selyanko et al. 2000; Tatulian et al. 2001).

KCNQ2+3 $V_{1/2}$ values showed a difference of 7 mV between tail and steady-state conductance analysis. Values of $V_{1/2}$ and k were similar to those described in prior publications (Selyanko et al. 2000; Suh and Hille 2007; Tatulian et al. 2001; Wickenden et al. 2007).

For KCNQ5 and KCNQ3+5, $V_{1/2}$ and k values were comparable to the literature (Jensen et al. 2007; Schroeder et al. 2000; Wickenden et al. 2001). Inactivation was much smaller in KCNQ3+5 expressed currents than observed with KCNQ5 alone. It was surprising to note that KCNQ3+5 cotransfection yielded the voltage dependence of activation to be in a more positive voltage range than those of its constituents. This might imply complex interaction effects between these different KCNQ channel subunits affecting the voltage sensors.

$V_{1/2}$ values found by Selyanko, Tatulian, Suh and Hille were 10 mV more positive than $V_{1/2}$ values determined in the course of this investigation. Factors explaining these differences might be the use of acetate as the negative ion used in the pipette solution by Selyanko and Tatulian as well as a lower extracellular potassium concentration. Acetate inside the pipette might lessen a Donnan potential error of approximately 10 mV of magnitude (Horn and Marty 1988) in perforated-patch. An additional shift in $V_{1/2}$ by a different $[K^+]_e$ might also play a role as their experiments were performed in 2.5 mM $[K^+]_e$ compared to 5 mM here.

Further differences in the results might be explained by the use of different expression systems, i.e. cDNA from different species and different magnitudes of current were measured. Different expression systems were used such as CHO-cells (Selyanko et al. 2000; Tatulian et al. 2001), HEK-TsA-201-cells (Suh and Hille 2007) and oocytes (Wang et al. 1998). KCNQ investigations were also performed with cDNA from different species. Whereas in my work human KCNQ2+3 heteromultimers were used others investigated heteromultimers from human KCNQ2

and rat KCNQ3 (Selyanko et al. 2000; Suh and Hille 2007; Tatulian et al. 2001). Another possible explanation is the magnitude of current measured with different series resistance and K^+ accumulation effects. In general, absolute values for $V_{1/2}$ and k of KCNQ activation show variability when comparing prior publications.

An increase in $[K^+]_e$ between 5 mM and 154 mM showed a reversible and significant shift in the voltage dependence of activation (chapter 4.3.1 and table 5). $V_{1/2}$ maximally shifted between -17.2 mV and -4.4 mV in the order KCNQ3+5 > KCNQ 2+3 > KCNQ2 > KCNQ5 > KCNQ3. Effects of extracellular K^+ accumulation as well as liquid junction potentials and Donnan potentials were considered. Simulation of a realistic residual series resistance after electronic compensation of 2 MΩ did show the voltage shift in activation to decrease with more than half of it still remaining after taking into account the residual uncompensated series resistance (chapter 4.4.4). The shift in voltage dependence of activation is confirmed by the results of acceleration in the time course of activation that is discussed in the next chapter (5.2.2).

Compared to the results at the node of Ranvier in rat rat sciatic nerves (Schwarz et al. 2006) the negative shift in voltage dependence of activation in increasing $[K^+]_e$ was smaller. I_{Ks} at the node of Ranvier showed a shift in voltage dependence of activation from about -23 mV to -62mV changing from ringer to 154 mM $[K^+]_e$ and is supposed to be carried by KCNQ2. Heterologously expressed KCNQ2 showed only a shift from -29 mV to -37 mV in the same range of $[K^+]_e$ change. A shift of -6.4 mV found in voltage dependence of activation for KCNQ2+3 when going from 5 to 40 mM $[K^+]_e$ was bigger than the results published (Suh and Hille 2007) which showed a difference of -1 mV going from 2.6 mM to 30 mM $[K^+]_e$. This difference in voltage shift might be explained by the use of differently expressed ion channels. In this investigation only human clones of KCNQ were expressed in CHO cells, whereas Suh and Hille used a chimera of human KCNQ2 and rat KCNQ3 coexpressed in HEK-TsA-201 cells. One publication showed a positive shift of +12 mV in voltage dependence of activation of M- current in bullfrog sympathetic neurons with increasing $[K^+]_e$ from 2.5 mM to 15 mM (Block and Jones 1996). A statistical significance of this positive shift was not mentioned in the publication and the number of experiments was small (n=5) with a notable standard error of 4 mV and 8 mV respectively.

A negative shift in the voltage dependence of activation has already been described for other potassium channels: HERG (Ho et al. 1998), rerg1, rerg3 (Sturm et al. 2005) and Kv4.3 (Wang et al. 2004). A possible mechanism suggested for Kv4.3 was a slowing of deactivation and stabilisation of the open state of the channel which might be caused by binding of K^+ ions to an extracellular binding site as was suggested for KCNQ1 (Yang and Sigworth 1998). A slowing of deactivation could be shown for KCNQ2+3 at membrane potentials negative to -80 mV in the course of this investigation.

An increase in the slope of voltage-dependent activation in raised $[K^+]_e$ was found when analysing tail currents but could not be confirmed when analysing steady-state conductance (fig. 14). An increase in the slope of the Boltzmann curve in tail current analysis can be explained by non-saturation of activation curves. As discussed in the previous chapter this is most probably caused by extracellular K^+ accumulation. The effect of this accumulation is stronger in low than in high extracellular K^+. Therefore fitting of the respective tail current activation curves seems to be shallower than it actually would be without K^+ accumulation.

Increasing $[K^+]_e$ showed a significant left shift in voltage dependence of activation in the KCNQ currents investigated, whereas an increase in the slope of activation was probably an artefact of measurement. The negative shift in half maximal activation is relatively small in experimental high $[K^+]_e$, but might be important when increasing K^+ currents around sensitive threshold potentials. The large change in $V_{1/2}$ found when increasing $[K^+]_e$ for I_{Ks} at the node of Ranvier (Schwarz et al. 2006) can only partially be explained by heterologously expressed KCNQ channels. Therefore, an additional mechanism must add to mediate the effects observed for native I_{Ks} when increasing $[K^+]_e$. It remains a matter of speculation if an additional β channel subunits might add to the magnitude of the effect found. This idea could be an approach to further experimentation in the future.

5.2.2 Time course of activation and deactivation

Kinetics of activation showed acceleration in higher $[K^+]_e$, whereas deactivation showed acceleration or slowing depending on membrane voltages and current size (fig. 10 and table 4).

KCNQ2+3 showed a significant increase in the rate of activation from holding potential to membrane potentials negative to +10 mV in 40 mM $[K^+]_e$, whereas acceleration due to $[K^+]_e$ rise became smaller and insignificant during depolarisation to more positive membrane potentials. This behaviour mimics that of the A-type current mediated by Kv4.3 which showed significant acceleration of activation to potentials negative to -10 mV due to a rise in $[K^+]_e$ from 2 mM to 98 mM (Wang et al. 2004). The change in time course of activation and deactivation of KCNQ2+3 found during this investigation is a new description of a change in kinetic behaviour caused by a rise in $[K^+]_e$ in a delayed rectifier type potassium channel. Prior investigation of KCNQ2+3 did not show any significant acceleration in kinetics (Suh and Hille 2007). These prior experiments investigated kinetics of activation from a holding potential of -60 mV depolarising to -20 mV in ion concentration changes between 2.5 mM and 30 mM $[K^+]_e$.

Voltage dependence of activation in the course of this experimental investigation shifted by about -10 mV from 5 mM to 154 mM $[K^+]_e$. Time constants of activation at $V_{1/2}$ in both high and low $[K^+]_e$ were at the same value of approximately 250 ms. This indicates that acceleration of activation to potentials between -40 mV and +10 mV could be explained by the negative shift in the voltage dependence of activation. This idea will be detailed below.

$$C \underset{\beta}{\overset{\alpha}{\rightleftharpoons}} O$$
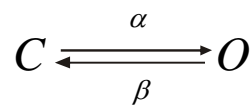
$$\tau = \frac{1}{\alpha + \beta} \Leftrightarrow \frac{1}{\tau} = \alpha + \beta$$

$$at \ V_m = V_{1/2}: \qquad \alpha = \beta \Rightarrow \tau = \max. \ (slowest)$$

In the experiments investigating the kinetics of KCNQ activation and deactivation only a limited range of membrane potentials was accessible by using the described pulse protocol (fig. 9). At each membrane potential there is an equilibrium between open (**O**) and closed (**C**) states of the ion channels. The rate of the transitions τ between these states can be defined as the reciprocal of the sum of the opening rate α and the closing rate β (see equations above). Upon depolarisation of the membrane

and thereby increasing the activation of channels, the opening rate α increases whereas the closing rate β decreases. The time constant τ reaches a maximum at $V_{1/2}$ and opening rate α and closing rate β are equal at this membrane potential. This has been described for the M-current in bullfrog sympathetic neurons (Adams et al. 1982). At this maximum of τ, when the membrane potential induces half maximal channel activation, the time constant attains its largest value. At both more positive and more negative potentials to $V_{1/2}$ channel transitions become faster (dashed curve in **fig. 22**).

Upon a negative shift in the voltage dependence of activation as found with increasing the extracellular potassium concentration, the bell shaped curve of τ in **fig. 22** shifts accordingly. This explains why time constants of activation and deactivation at the membrane potentials investigated show an acceleration comparing the time constants at a particular membrane potential with rising extracellular potassium concentration. Time constants investigated were eligible to exponential fitting (chapter 4.3.2) and showed only an excerpt (**fig. 22 inset**) of the whole range of membrane potentials (**fig. 22** dashed curves).
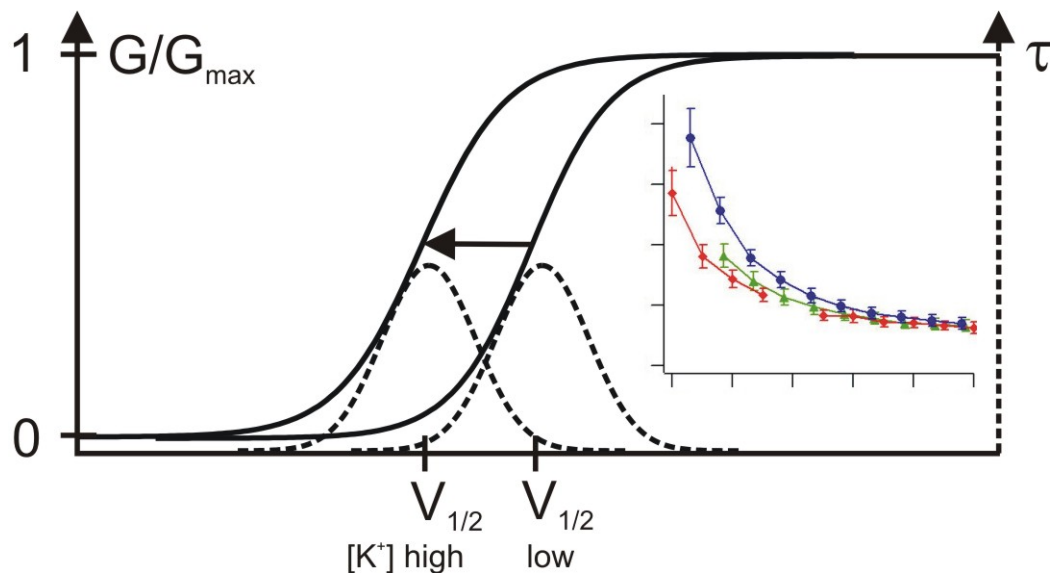
Fig. 22: A shift in the voltage dependence of channel gating results in a change in the kinetics of the macroscopic current
Voltage dependence of KCNQ ion conduction (G) is shown normalized to maximal conduction G_{max}. The voltage of half maximal activation $V_{1/2}$ is shifted to more negative potentials in higher extracellular potassium concentrations. The rate of channel transitions τ (dotted line) is at a maximum at $V_{1/2}$. An acceleration of the rate of activation in higher $[K^+]_e$ respective to a fixed membrane potential, is a consequence of the shift in voltage dependence of channel activation. The inset shows the experimental found acceleration of time constants of activation for KCNQ2+3 at different membrane potentials in rising $[K^+]_e$ already described in chapter 4.3.2. Figure adapted from fig. 16 (Adams et al. 1982).

This excerpt gives the impression of an acceleration of channel activation, whereas only the distribution relative to the membrane potential is shifted.

Deactivation on the other hand showed significant slowing at potentials negative to -80 mV and acceleration at potentials positive to -40 mV (fig. 10). There was no significant change in the time course of deactivation at around -60 mV as has been described for KCNQ2+3 (Suh and Hille 2007). Slowing of deactivation has been described for Kv4.3 in rising $[K^+]_e$ (Wang et al. 2004) over the whole potential range. Contrary to Kv4.3, KCNQ2+3 showed acceleration of deactivation to potentials positive to -40 mV. This might again be a result of the shift in voltage dependence as explained above for activation.

On the contrary, slowing of deactivation to potentials negative to -80 mV might be an artefact caused by series resistance. As the $[K^+]_e$ rises repolarising to negative membrane potentials results in high inward currents which can be seen in fig. 9. This causes an increasing voltage clamp error for these negative membrane potentials in high $[K^+]_e$ making the time course of deactivation to appear slower than it actually was.

In summary an acceleration of activation and deactivation to membrane potentials positive to -40 mV in high $[K^+]_e$ can be explained by and confirms the negative shift in voltage dependence of KCNQ channel activation in rising $[K^+]_e$.

5.2.3 Increase in KCNQ conductance with rises in $[K^+]_e$

Calculation of steady-state whole-cell conductance at different membrane potentials showed that KCNQ conductance did almost double when going from ringer to 154 mM $[K^+]_e$ (fig. 12 and fig. 13). This could be either due to intrinsic properties of KCNQ channels or to an extrinsic effect on the cell and experimental system.

An extrinsic explanation of this observation might be a non-specific increase in membrane conductance due to an increase in leak conductance mediated by endogenous CHO ion channels or due to Nystatin diffusing laterally out of the patch. A linear, non-voltage-dependent linear leak was corrected for in conductance calculations in the course of this investigation and therefore improbably the cause. And Nystatin has not shown to laterally diffuse away from the patch (Horn 1991). Control experiments changing back to the initial low $[K^+]_e$ showed reversibility of this effect speaking against the idea of Nystatin diffusing into the whole cell membrane. Thus, the increase in membrane conductance is more likely to be an intrinsic property of the specific KCNQ current.

An increase in whole-cell conductance was similar for KCNQ2, KCNQ3 and KCNQ2+3 in 40 mM $[K^+]_e$ but KCNQ2 did show decreased conductance in 156 mM $[K^+]_e$ contrary to KCNQ3 and KCNQ2+3. This might be explained by current rundown as decreasing $[K^+]_e$ back to 5 mM recovery controls showed decreased conductance for KCNQ2 when compared to the initial conductance amplitude.

Possible intrinsic mechanisms for increasing whole-cell conductance might be an increase in open probability, single channel KCNQ conductance or a change in number of channels in the membrane.

First an increase in channel open probability with increasing $[K^+]_e$ would be consistent with findings of a negative shift in the voltage dependence of activation and acceleration of activation. Open probability P_o of activation at 0 mV studied in single channel recordings was much higher for KCNQ3 (P_o=0.59) compared to KCNQ2 (P_o=0.15) and KCNQ2+3 (P_o=0.30) in low $[K^+]_e$ (Selyanko et al. 2001). A doubling of conductance explained by a doubling in P_o is possible for KCNQ2 and KCNQ2+3 but P_o for KCNQ3 is already 60% in low $[K^+]_e$. As KCNQ3 showed the highest increase in whole-cell conductance an increase in P_o is unlikely to be the only mechanism causing an increase in conductance.

A second explanation for an increase in whole-cell conductance might be an increase in single channel conductance caused by a $[K^+]_e$ rise. An increase in conductance has early been described for the delayed rectifier current I_{Kr} in rabbit nodal heart cells (Shibasaki T. 1987) which is now known to be mediated by erg1 channels and results predominantly from an increase in single channel conductance (Kiehn et al. 1996). This might also be true for KCNQ channels as several conductance states have been suggested for KCNQ1 chimera (Yang and Sigworth 1998) and KCNQ2+3 (Selyanko et al. 2001). A chimera of rat mink β-subunit with human KCNQ1 showed a higher single channel conductance with a rise in $[K^+]_e$ to 10 mM. An additional conductance state has already been described for KCNQ2+3 showing a lower single channel conductance. This is contrary to my findings showing an increase in whole-cell conductance in rising $[K^+]_e$. An idea explaining an increase in single channel conductance might be due to an intrinsic K^+ sensing mechanism of KCNQ or linked to a K^+ sensible messenger system modulating KCNQ conductance, e.g. PIP_2 (Suh and Hille 2002).

A third explanation might be a rapid insertion and removal of channels into and out of the membrane from sub-membranous stores triggered by a $[K^+]_e$ sensitive mechanism. This is improbable as although this mechanism of channel current regulation is known, it might be too slow for the changes in conductance described for KCNQ here.

In summary a rise in $[K^+]_e$ showed a left shift in voltage dependence of activation, an acceleration of activation and deactivation in the investigated voltage range and an increase in whole-cell conductance. In the future single channel recordings in rising $[K^+]_e$ might advance the understanding of the mechanism causing these changes in biophysical properties of KCNQ channels.

5.3 Physiological and pathophysiological implications

KCNQ channels are expressed in various cells in the central and the peripheral nervous system including dorsal root ganglia (Tokimasa and Akasu 1990) and hippocampal neurons (Selyanko et al. 2001). Especially heteromeric KCNQ2+3 channels are the molecular correlate of the functionally important M-channels (Wang et al. 1998) as well as KCNQ3+5 heteromultimeric channels (Schroeder et al. 2000). The M-current has an effect on the control of neuronal excitability and its function was early described by one of its discoverers (Adams et al. 1982) as an exertion of "potential clamping on the cell membrane when attempts are made to displace it from rest potential".

Characteristic for exerting this function is the early activation with little or no inactivation of the M-current at sub-threshold membrane potentials. KCNQ channels activate at potentials negative to the threshold potential and therefore exert a pivotal control over neuronal excitability and response patterns by attenuating repetitive AP discharges (Pongs 2007). The magnitude of this excitability controlling current can be adapted by neurotransmitters such as acetylcholine. Mutations in the KCNQ gene can lead to a heritable form of epilepsy (benign familial neonatal convulsions - BFNC) when the M-channels lose their function as a "break" on neuronal excitability (Jentsch 2000).

The described left-shift in voltage dependence of activation with an acceleration of activation and an increase in conductance might increase these functions of KCNQ

currents in conditions with elevated $[K^+]_e$ and thereby might counteract an hyperexcitable state of the neuron.

The change in biophysical properties of KCNQ currents were found to appear with a drastic rise in $[K^+]_e$ from 5 mM to 40 mM and 154 mM under experimental conditions. In vivo $[K^+]_e$ is tightly controlled below a so-called 'ceiling' level of 10 mM $[K^+]_e$ even under conditions of extreme neuronal firing and hyperactivity (Benninger et al. 1980; Heinemann and Dietzel 1984; Heinemann and Lux 1977; Xiong and Stringer 1999). A more important rise in $[K^+]_e$ of up to 50 to 80 mM has been described for conditions of spreading depression (Kager et al. 2000; Somjen 2001; Somjen 2002) and brain ischemia (Leis et al. 2005).

Under the assumption that the found effects on KCNQ activation are also present in vivo and in the physiological range of a $[K^+]_e$ rise, the changes in KCNQ's biophysical properties described here might increase its function in regulating the resting membrane potential and counteracting hyperexcitability under conditions of raised $[K^+]_e$.

A change in the characteristics of KCNQ channel activation as has been found during this investigation might be one component of "fine-tuning" its physiological function by adapting the magnitude of KCNQ currents to conditions of elevated $[K^+]_e$. Furthermore these effects might be even more evident under pathophysiological conditions such as epileptic seizures, spreading depression or brain ischemia with a more important rise in $[K^+]_e$.

6   SUMMARY

In the course of this investigation, properties of human KCNQ channels were investigated in different extracellular potassium concentrations (5 mM, 40 mM and 154 mM). Neuronal channel subunits and subunit compositions (KCNQ2, KCNQ3, KCNQ5, KCNQ2+3, KCNQ3+5) were heterologously expressed in CHO cells and analyzed in electrophysiological experiments using the patch-clamp technique. Biophysical properties of KCNQ channel current changed in elevated with respect to physiological extracellular potassium concentrations of 5 mM in the following manner:

- A significant shift in voltage dependence of activation between 4-7 mV to more negative potentials could be found in 40 mM $[K^+]_e$ for KCNQ2, KCNQ3 and KCNQ2+3

- A significant shift in voltage dependence of activation between 7-17 mV to more negative potentials could be found in 154 mM $[K^+]_e$ for all KCNQ channels

- A significant acceleration of activation and deactivation in 40 and 154 mM at potentials positive to -40 mV

- A slowing in deactivation at potentials negative to -80 mV

- An increase in whole-cell conductance could be found in all elevated $[K^+]_e$

Methodological difficulties were investigated in order to correctly evaluate and interpret the outcome of the experiments in increasing extracellular potassium concentrations:

- Amplitude and duration of potassium currents changed the potassium reversal potential during voltage-clamp experiments

- The method of either analysing tail-currents or sustained-currents affected the interpretation of voltage dependence of activation

- Series resistance errors remaining after electronic compensation could not be neglected in non-inactivating, experimentally overexpressed KCNQ-channel-currents

The described changes in biophysical properties of KCNQ channels in increasing extracellular potassium concentration could be a mechanism to adapt the controlling function of KCNQ currents on cellular excitability in states such as repetitive neuronal firing and brain ischemia.

7   REFERENCES

ADAMS P.R., BROWN D.A. and CONSTANTI A. (**1982**); M-currents and other potassium currents in bullfog sympathetic neurons; *The Journal of Physiology Online;* 330: 537-572

ASHCROFT F.M. (**2000**); Ion Channels and Disease; *Academic Press;* Chapter 6: p.97-124

ASHCROFT F.M. (**2006**); From molecule to malady; *Nature;* 440: 440-447

BARRY P.H. and LYNCH J.W. (**1991**); Liquid junction potentials and small cell effects in patch-clamp analysis; *Journal of Membrane Biology;* 121: 101-117

BENNINGER C., KADIS J. and PRINCE D.A. (**1980**); Extracellular calcium and potassium changes in hippocampal slices; *Brain Research;* 187: 165-182

BIERVERT C., SCHROEDER B.C., KUBISCH C., BERKOVIC S.F., PROPPING P., JENTSCH T.J. and STEINLEIN O.K. (**1998**); A Potassium Channel Mutation in Neonatal Human Epilepsy; *Science;* 279: 403-406

BLOCK and JONES (**1996**); Ion Permeation and Block of M-Type and Delayed Rectifier Potassium Channels - Whole-Cell Recordings from Bullfrog Sympathetic Neurons; *The Journal of General Physiology;* 107: 473-488

BROWN D.A. and GAYLE M. (**2009**); Neural KCNQ (Kv7) channels; *British Journal of Pharmacology;* 156: 1185-1195

CHEN J.W.Y. and EATOCK R.A. (**2000**); Major Potassium Conductance in Type I Hair Cells From Rat Semicircular Canals: Characterization and Modulation by Nitric Oxide; *Journal of Neurophysiology;* 84: 139-151

COOPER E., ALDAPE K., ABOSCH A., JAN Y. and JAN L. (**2000**); Colocalization and coassembly of two human brain M-type potassium channel subunits that are mutated in epilepsy; *Proc Natl Acad Sci U S A;* 97: 4914-4919

DELMAS P. and BROWN D.A. (**2005**); Pathways modulating neural KCNQ/M (Kv7) potassium channels; *Nat Rev Neurosci;* 6: 850-862

GAMPER N., STOCKAND J. and SHAPIRO M. (**2005**); The use of Chinese hamster ovary (CHO) cells in the study of ion channels; *Journal of Pharmacological and Toxicological Methods;* 51: 177-185

GAMPER N. and SHAPIRO M.S. (**2003**); Calmodulin Mediates Ca2+-dependent Modulation of M-type K+ Channels; *The Journal of General Physiology;* 122: 17-31

GILANYI M., IKRENYI C., FEKETE J., IKRENYI K. and KOVACH A.G. (**1988**); Ion concentrations in subcutaneous interstitial fluid: measured versus expected values; *AJP - Renal Physiology;* 255: F513-F519

HAMILL O.P., MARTY A., NEHER E., SAKMANN B. and SIFWORTH F.J. (**1981**); Improved patch-clamp techniques for high-resolution current recording from cells and cell-free membrane patches; *Pflügers Archly;* 39: 85-100

HANSEN H.H., WAROUX O., SEUTIN V., JENTSCH T.J., AZNAR S. and MIKKELSEN J.D. (**2008**); Kv7 channels: interaction with dopaminergic and serotonergic neurotransmission in the CNS; *The Journal of Physiology;* 586: 1823-1832

HEINEMANN U. and DIETZEL I. (**1984**); Extracellular potassium concentration in chronic alumina cream foci of cats; *Journal of Neurophysiology;* 52: 421-434

HEINEMANN U. and LUX H. (**1977**); Ceiling of stimulus-induced rises in extracellular potassium concentration in the cerebral cortex of cats.; *Brain Research;* 120: 231-249

HILLE B. and SCHWARZ W. (**1978**); Potassium channels as multi-ion single-file pores; *The Journal of General Physiology;* 72: 409-442

HILLE B. (**2001**); Ion Channels of Excitable Membranes (3rd); *Sinauer Associates Inc.,U.S.;* Chapter 10: p.315-319

HO W.K., KIM I., LEE C.O. and EARM Y.E. (**1998**); Voltage-dependent blockade of HERG channels expressed in Xenopus oocytes by external Ca2+ and Mg2+; *The Journal of Physiology Online;* 507: 631-638

HORN R. and MARTY A. (**1988**); Muscarinic activation of ionic currents measured by a new whole-cell recording method; *The Journal of General Physiology;* 92: 145-159

HORN R. (**1991**); Estimating the number of channels in patch recordings; *Biophysical Journal;* 60: 433-439

HORN R. and KORN S.J. (**1992**); Prevention of Rundown in Electrophysiological Recording; *Methods in Enzymology: Volume 207: Ion Channels by Academic Press Inc., U.S.;* Chapter 8: p. 152-155

JENSEN H.S., GRUNNET M. and OLESEN S.P. (**2007**); Inactivation as a New Regulatory Mechanism for Neuronal Kv7 Channels; *Biophysical Journal;* 92: 2747-2756

JENTSCH T.J. (**2000**); Neuronal KCNQ potassium channels: physiology and role in disease.; *Nat Rev Neurosci;* 1: 21-30

KAGER H., WADMAN W.J. and SOMJEN G.G. (**2000**); Simulated Seizures and Spreading Depression in a Neuron Model Incorporating Interstitial Space and Ion Concentrations; *Journal of Neurophysiology;* 84: 495-512

KIEHN J., LACERDA A.E., WIBLE B. and BROWN A.M. (**1996**); Molecular Physiology and Pharmacology of HERG: Single-Channel Currents and Block by Dofetilide; *Circulation;* 94: 2572-2579

KORSGAARD M.P.G., HARTZ B.P., BROWN W.D., AHRING P.K., STROBAEK D. and MIRZA N.R. (**2005**); Anxiolytic Effects of Maxipost (BMS-204352) and Retigabine via Activation of Neuronal Kv7 Channels; *Journal of Pharmacology And Experimental Therapeutics;* 314: 282-292

KUBISCH C., SCHROEDER B.R.C., FRIEDRICH T., L³TJOHANN B.R., EL AMRAOUI A., MARLIN S., PETIT C. and JENTSCH T.J. (**1999**); KCNQ4, a Novel Potassium Channel Expressed in Sensory Outer Hair Cells, Is Mutated in Dominant Deafness; *Cell;* 96: 437-446

KUFFLER S.W., NICHOLLS J.G. and ORKAND R.K. (**1966**); Physiological properties of glial cells in the central nervous system of amphibia; *Journal of Neurophysiology;* 29: 768-787

LEIS J., BEKAR L. and WALZ W. (**2005**); Potassium homeostasis in the ischemic brain; *Glia;* 50: 407-416

LI X., SHIMADA K., SHOWALTER L.A. and WEINMAN S.A. (**2000**); Biophysical Properties of ClC-3 Differentiate It from Swelling-activated Chloride Channels in Chinese Hamster Ovary-K1 Cells; *Journal of Biological Chemistry;* 275: 35994-35998

MARTY A. and NEHER E. (**1983**); Tight-seal whole-cell recording; *Single Channel Recording by B.Sakmann and E.Neher, Plenum Publishing Corp., New York;* Chapter 2: p.31-51

MUNRO G., ERICHSEN H.K. and MIRZA N.R. (**2007**); Pharmacological comparison of anticonvulsant drugs in animal models of persistent pain and anxiety; *Neuropharmacology;* 53: 609-618

NEHER E. (**1992**); Correction for Liquid Junction Potentials in Patch Clamp Experiments; *Methods in Enzymology: Ion Channels: 207;* Chapter 6: p. 123-131

NEYROUD N., TESSON F., DENJOY I., LEIBOVICI M., DONGER C., BARHANIN J., FAURE S., GARY F., COUMEL P., PETIT C., SCHWARTZ K. and GUICHENEY P. (**1997**); A novel mutation in the potassium channel gene KVLQT1 causes the Jervell and Lange-Nielsen cardioauditory syndrome; *Nat Genet;* 15: 186-189

NG B. and BARRY P.H. (**1995**); The measurement of ionic conductivities and mobilities of certain less common organic ions needed for junction potential corrections in electrophysiology; *Journal of Neuroscience Methods;* 56: 37-41

NICHOLS J., MARTIN R. and WALLACE B. (**1995**); Ionale Basis des Ruhemembranpotentials; *Vom Neuron zum Gehirn;* Chapter 3: p.46-50

NOBLE D. (**2008**); The Music of Life: Biology Beyond Genes; *Oxford University Press;* Chapter 5: p.55-67

NUMBERGER M. and DRAGUHN A. (**1996**); Patch-Clamp-Technik; *Spektrum Akademischer Verlag;*

ORKAND R.K., NICHOLLS J.G. and KUFFLER S.W. (**1966**); Effect of nerve impulses on the membrane potential of glial cells in the central nervous system of amphibia; *Journal of Neurophysiology;* 29: 788-806

PASSMORE G.M., SELYANKO A.A., MISTRY M., AL QATARI M., MARSH S.J., MATTHEWS E.A., DICKENSON A.H., BROWN T.A., BURBIDGE S.A., MAIN M. and BROWN D.A. (**2003**); KCNQ/M Currents in Sensory Neurons: Significance for Pain Therapy; *Journal of Neuroscience;* 23: 7227-7236

PFAFFINGER P. (**1988**); Muscarine and t-LHRH suppress M-current by activating an IAP- insensitive G-protein; *Journal of Neuroscience;* 8: 3343-3353

PONGS O. (**2007**); Regulation of Excitability by Potassium Channels; *Results Probl Cell Differ;* 44: 145-161

PORTER R.J., PARTIOT A., SACHDEO R., NOHRIA V., ALVES W.M. and ON BEHALF OF THE (**2007**); Randomized, multicenter, dose-ranging trial of retigabine for partial-onset seizures; *Neurology;* 68: 1197-1204

PROLE D.L. and MARRION N.V. (**2004**); Ionic Permeation and Conduction Properties of Neuronal KCNQ2/KCNQ3 Potassium Channels; *Biophysical Journal;* 86: 1454-1469

PUCK T.T., CIECIURA S.J. and ROBINSON A. (**1958**); Genetics of somatic mammalian cells. III. Long-term cultivation of euploid cells from human and animal subjects; *The Journal of Experimental Medicine;* 10: 945-956

PUNKE M.A. and FRIEDERICH P. (**2007**); Amitriptyline Is a Potent Blocker of Human Kv1.1 and Kv7.2/7.3 Channels; *Anesthesia Analgesia;* 104: 1256-1264

ROBBINS J. (**2001**); KCNQ potassium channels: physiology, pathophysiology, and pharmacology; *Pharmacology & Therapeutics;* 90: 1-19

SCHROEDER B.C., HECHENBERGER M., WEINREICH F., KUBISCH C. and JENTSCH T.J. (**2000**); KCNQ5, a Novel Potassium Channel Broadly Expressed in Brain, Mediates M-type Currents; *Journal of Biological Chemistry;* 275: 24089-24095

SCHWARZ J.R., GLASSMEIER G., COOPER E.C., KAO T.C., NODERA H., TABUENA D., KAJI R. and BOSTOCK H. (**2006**); KCNQ channels mediate IKs, a slow K+ current regulating excitability in the rat node of Ranvier; *The Journal of Physiology Online;* 573: 17-34

SELYANKO A.A. and BROWN D.A. (**1996**); Intracellular Calcium Directly Inhibits Potassium M Channels in Excised Membrane Patches from Rat Sympathetic Neurons; *Neuron;* 16: 151-162

SELYANKO A.A., HADLEY J.K. and BROWN D.A. (**2001**); Properties of single
M-type KCNQ2/KCNQ3 potassium channels expressed in mammalian cells;
The Journal of Physiology Online; 534: 15-24

SELYANKO A.A., HADLEY J.K., WOOD I.C., ABOGADIE F.C., JENTSCH T.J.
and BROWN D.A. (**2000**); Inhibition of KCNQ1-4 potassium channels
expressed in mammalian cells via M1 muscarinic acetylcholine receptors;
The Journal of Physiology Online; 522: 349-355

SHIBASAKI T. (**1987**); Conductance and kinetics of delayed rectifier potassium
channels in nodal cells of the rabbit heart; *The Journal of Physiology Online;*
387: 227-250

SOMJEN G.G. (**2001**); Mechanisms of Spreading Depression and Hypoxic
Spreading Depression-Like Depolarization; *Physiological Reviews;* 81: 1065-
1096

SOMJEN G.G. (**2002**); Ion Regulation in the Brain: Implications for
Pathophysiology; *The Neuroscientist;* 8: 254-267

STURM P., WIMMERS S., SCHWARZ J.R. and BAUER C.K. (**2005**); Extracellular
potassium effects are conserved within the rat erg K+ channel family; *The
Journal of Physiology Online;* 564: 329-345

SUH B.C. and HILLE B. (**2002**); Recovery from Muscarinic Modulation of M
Current Channels Requires Phosphatidylinositol 4,5-Bisphosphate Synthesis;
Neuron; 35: 507-520

SUH B.C. and HILLE B. (**2007**); Electrostatic Interaction of Internal Mg2+ with
Membrane PIP2 Seen with KCNQ K+ Channels; *The Journal of General
Physiology;* 130: 241-256

SUH B.C., HOROWITZ L.F., HIRDES W., MACKIE K. and HILLE B. (**2004**);
Regulation of KCNQ2/KCNQ3 Current by G Protein Cycling: The Kinetics

of Receptor-mediated Signaling by Gq; *The Journal of General Physiology;* 123: 663-683

TATULIAN L., DELMAS P., ABOGADIE F.C. and BROWN D.A. (**2001**); Activation of Expressed KCNQ Potassium Currents and Native Neuronal M-Type Potassium Currents by the Anti-Convulsant Drug Retigabine; *Journal of Neuroscience;* 21: 5535-5545

TOKIMASA T. and AKASU T. (**1990**); ATP regulates muscarine-sensitive potassium current in dissociated bull-frog primary afferent neurones; *The Journal of Physiology Online;* 426: 241-264

TRAUNER (**2009**); Potassium Channels: Symmetric, Selective, and Sensitive; *Angewandte Chemie International Edition;* 42: 5671-5675

VACA L. and SAMPIERI A. (**2002**); Calmodulin Modulates the Delay Period between Release of Calcium from Internal Stores and Activation of Calcium Influx via Endogenous TRP1 Channels; *Journal of Biological Chemistry;* 277: 42178-42187

VENTER J.C. et al. (**2001**); The Sequence of the Human Genome; *Science;* 291: 1304-1351

WANG H.S., PAN Z., SHI W., BROWN B.S., WYMORE R.S., COHEN I.S., DIXON J.E. and MCKINNON D. (**1998**); KCNQ2 and KCNQ3 Potassium Channel Subunits: Molecular Correlates of the M-Channel; *Science;* 282: 1890-1893

WANG S., BONDARENKO V.E., QU Y., MORALES M.J., RASMUSSON R.L. and STRAUSS H.C. (**2004**); Activation properties of Kv4.3 channels: time, voltage and [K+]o dependence; *The Journal of Physiology Online;* 557: 705-717

WICKENDEN A.D., KRAJEWSKI J.L., LONDON B., WAGONER P.K., WILSON W.A., CLARK S., ROELOFFS R., MCNAUGHTON-SMITH G. and

RIGDON G.C. (**2007**); ICA-27243: A novel, selective KCNQ2/Q3 potassium channel activator; *Molecular Pharmacology;* mol-

WICKENDEN A.D., ZOU A., WAGONER P.K. and JEGLA T. (**2001**); Characterization of KCNQ5/Q3 potassium channels expressed in mammalian cells; *Br J Pharmacol;* 132: 381-384

XIONG Z.Q. and STRINGER J.L. (**1999**); Astrocytic regulation of the recovery of extracellular potassium after seizures in vivo; *European Journal of Neuroscience;* 11: 1677-1684

YANG Y. and SIGWORTH F.J. (**1998**); Single-Channel Properties of IKs Potassium Channels; *The Journal of General Physiology;* 112: 665-678

ZHANG H., CRACIUN L.C., MIRSHAHI T., ROHACS T., LOPES C.M.B., JIN T. and LOGOTHETIS D.E. (**2003**); PIP2 Activates KCNQ Channels, and Its Hydrolysis Underlies Receptor-Mediated Inhibition of M Currents; *Neuron;* 37: 963-975

8   ACKNOWLEDGEMENTS

9   CURRICULUM VITAE

Arne Christoph Volker BILET, Date of Birth 27/6/1982

EDUCATION

2002 – 2009	**Hamburg School of Medicine**, Hamburg University, Germany
	Doctor of Medicine MD (6/2009)
2005 – 2007	**Center for Molecular Neurobiology** (ZMNH), Hamburg
	Graduate Studies in Molecular Biology - Diploma
2004 – 2005	**Université Victor Segalen**, Bordeaux, France
	School of Medicine, ERASMUS Scholar
2002 – 2004	**Center of Experimental Medicine**, University of Hamburg, Germany
	Degree in Molecular Medicine
2000 – 2002	**Fire Department of Hamburg**, Germany
	Rettungssanitäter, Rettungsassistent (Paramedic)
1998 – 2000	**St. Andrew's College**, Dublin, Republic of Ireland
	Bilingual International Baccalaureat Diploma

CAREER-RELATED EXPERIENCE

2009	**Universidade de São Paulo, Brasil:** Hepatology
2008	**Institute of Neurology, University College London:** Clinical Neurology
	Université Lausanne: General Surgery
	Université Bordeaux: Internal Medicine
2005	**Hôpital St. André Bordeaux:** Internal Medicine
	Hôpital Pellegrin Bordeaux: Orthopedics
	Hôpital Haut-Levêque Bordeaux: Gastroenterology
2004	**Philips Medical Systems:** Marketing X-ray products
2003	**Centre Hospitalier Universitaire Rouen:** Nursing Internship
2002	**University Heart Center Dresden:** ICU and OR Internship
	Krankenhaus Dresden Friedrichstadt: ER Internship
2001	**Feuer- und Rettungswache Altona, Hamburg:** Civil Service as Paramedic
1998	**German Electron Synchrotron Radiation Laboratory (DESY):**
	Internship in electronics at a particle acceleration facility
	Lufthansa Technik AG: Internship in plane mechanics and flight electronics

Hamburg, 3/1/2010

10   DECLARATION

I hereby declare that this submission is my own work and that, to the best of my knowledge and belief, it contains no material previously published or written by another person nor material which to a substantial extent has been accepted for the award of any other degree or diploma of the university or other institute of higher learning, except where due acknowledgment has been made in the text.

Hamburg, 3/1/2010

Arne Bilet

Eidesstattliche Versicherung:

Ich versichere ausdrücklich, dass ich die Arbeit selbständig und ohne fremde Hilfe verfasst, andere als die von mir angegebenen Quellen und Hilfsmittel nicht benutzt und die aus den benutzten Werken wörtlich oder inhaltlich entnommenen Stellen einzeln nach Ausgabe (Auflage und Jahr des Erscheinens), Band und Seite des benutzten Werkes kenntlich gemacht habe.

Ferner versichere ich, dass ich die Dissertation bisher nicht einem Fachvertreter an einer anderen Hochschule zur Überprüfung vorgelegt oder mich anderweitig um Zulassung zur Promotion beworben habe.

Hamburg, 3/1/2010

Arne Bilet